E12-10-006A

Dihadron Electroproduction in DIS with Transversely Polarized ^{3}He Target at 11 and 8.8 GeV

June 2, 2014

(A Proposal to Jefferson Lab (PAC 42))

J. Huang, X. Qian
Brookhaven National Laboratory, Upton, NY, 11973

H. Yao
College of William & Mary, Williamburg, VA

I. Akushevich, P.H. Chu, **H. Gao** (co-spokesperson), M. Huang, X. Li, G. Laskaris, M. Meziane, C. Peng, W. Xiong, X.F. Yan, Z. Ye, Y. Zhang
Duke University and TUNL, Durham, NC

P. Markowitz
Florida International University, Miami, FL

C. Chen, E. Christy, N. Kalantarians
Hampton University, Hampton, VA

H.J. Lu, X.H Yan
Huangshan University, Huangshan, P. R. China

Anselm Vossen
Indiana University, Bloomington, IN

H. Avakian, A. Camsonne, **J.-P. Chen** (co-spokesperson), E. Chudakov, S. Covrig, M. Dalton, A. Deur, J. Gomez, D. W. Higinbotham, J. O. Hansen, C. Keppel, R. Michaels, Y. Qiang
Jefferson Lab, Newport News, VA

X. Jiang
Los Alamos National Laboratory, Los Alamos, NM

K. Allada
Massachusetts Institute of Technology, Cambridge, MA

G. Dodge, L. EL Fassi, C.E. Hyde, S. Kuhn, L. Weinstein, Z. W. Zhao
Old Dominion University, Norfolk, VA

J. Beričič, M. Mihovilovič, S. Širca, S. Štajner
Jožef Stefan Institute, Ljubljana, Slovenia

P. Souder, R. Holmes
Syracuse University, Syracuse, NY

Z.-E. Meziani, M. Paolone and N. Sparveris
Temple University, Philadelphia, PA

X. Huang, L. Shi, Y. Wang, **Z. Xiao** (co-spokesperson), P. Zhuang
Tsinghua University, Beijing, China

A. Kotzinian
Yerevan Physics Institute, Yerevan, Armenia and INFN, Sezione di Torino, Torino, Italy

A. Courtoy (co-spokesperson)
Universite de Liege (ULg), Liege, Belgium and
INFN Laboratori Nazionali di Frascati, Frascati, Italy

A. Bacchetta, B. Pasquini, M. Radici
Universita' di Pavia and INFN Sezione di Pavia, Pavia, Italy

S. Scopetta
University of Perugia, and Istituto Nazionale di Fisica Nucleare, Sezione di Perugia, Perugia, Italy

A. Puckett, P. Schweitzer
University of Connecticut, Storrs, CT

L.P. Kaptari
Bogoliubov Laboratory of Theoretical Physics, JINR, Dubna, Russia

G. Salme'
Istituto Nazionale di Fisica Nucleare, Sezione di Roma, Roma, Italy

E. Pace
Physics Department, University of Rome Tor Vergata and Istituto Nazionale di Fisica Nucleare, Sezione di Tor Vergata, Roma, Italy

H. Matevosyan, **A. W. Thomas** (co-spokesperson)
CSSM and CoEPP, University of Adelaide, North Tce, Adelaide SA 5005, Australia

T. Badman, E. Long, K. Slifer, R. Zielinski
University of New Hampshire, Durham, NH

D. Crabb, D. Day, C. Gu, D. Keller, J. Liu, R. A. Oscar,
P. Peng, V. Sulkosky, S. Tkachenko, **J. Zhang** (spokesperson, Contact)
University of Virginia, Charlottesville, VA

Abstract

We propose to measure the **single target spin asymmetries (SSA)** of dihadron production in deep inelastic scattering (DIS) region using 11 and 8.8 GeV electron beam on a transversely polarized ^{3}He target. The Solenoidal Large Intensity Device (SoLID) in Hall A will be used to simultaneously detect the scattering electrons and the two charged pions ($\pi^+\pi^-$) in the reaction of $^3\mathbf{He}^{\uparrow}(e, e'\pi^+\pi^-)\mathbf{X}$, allowing us to map the SSA in a 4-D space of x, Q^2, $z_{\pi^+\pi^-}$ and $M_{\pi^+\pi^-}$. The asymmetries for the neutron can then be extracted after correcting the proton contribution and nuclear effects. Assuming leading twist dominance, the transversity distribution, h_1, can be extracted from the $\sin(\phi_R + \phi_S)$ modulation of the SSA combining with the world data on dihadron fragmentation functions. These data will provide crucial inputs to the flavor separation of the transversity, especially the d quark distribution, and therefore on the determination of the tensor charge of the nucleon. The wide range and precision data also allow us to check the validity of the factorization in dihadron process. Also, a possible Sivers effect in dihadron production in DIS will be investigated through the $\sin(\phi_R - \phi_S)$ and $\sin(\phi_T - \phi_S)$ modulations. This experiment will run simultaneously with the already approved experiment E12-10-006, which focuses on measuring the SSA through semi-inclusive pion electro-production (single pion). A total beam time of 90 days will be shared.

Contents

1 Introduction

The distribution of quarks and gluons inside hadrons can be described by means of parton distribution functions (PDFs). In a parton-model picture, PDFs describe combinations of number densities of quarks and gluons in a fast-moving hadron. The knowledge of PDFs is crucial for our understanding of Quantum Chromodynamics (QCD) and for the interpretation of high-energy experiments involving hadrons.

In the Bjorken limit the partonic structure of the nucleon is described, at leading-twist, by three PDFs: the well known unpolarized distribution functions $f_1^q(x)$; and helicity distribution functions $g_1^q(x)$; and the transversity distribution function $h_1^q(x)$, which measures the distribution of transversely polarized quarks of flavor q and fractional momentum x in a transversely polarized nucleon [1, 2, 3]. Intuitively, helicity and transversity give two orthogonal pictures of the partonic structure of polarized nucleons. They have very different properties, and transversity is poorly known. We propose here to study a target spin asymmetry in dihadron production that can be used to extract the transversity distribution, using an 8.8 and 11 GeV electron beam from the upgraded CEBAF facility and the SoLID detector equipped with a transversely polarized target.

Transversity arises from the interference of amplitudes with different parton and parent nucleon helicities. In jargon, it is called a chiral-odd function. There is no transversity for gluons in a nucleon, and h_1^q evolves with Q^2 as a pure non-singlet [4]. From transversity one can build the nucleon tensor charge, that can also be computed in lattice QCD [5] (for a review on transversity, see Ref. [6] and references therein). The value of tensor charge is predicted by some models to place constraints on some extensions of the Standard Model, e.g. [7].

Transversity is particularly difficult to measure because it must appear in cross sections combined with another chiral-odd function. The simplest example is the cross section of the transversely polarized Drell-Yan process, where h_1^q appears multiplied by its antiquark partner $h_1^{\bar{q}}$ [1, 3]. At present, there exists no measurement of this process.

Another example is the cross section for semi-inclusive Deep Inelastic Scattering (DIS),

$$\ell(l) + N(P) \to \ell(l') + H(P_h) + X \quad ,$$

where h_1^q appears in a convolution with the chiral-odd Collins fragmentation function $H_1^{\perp q}$ [8], which describes the correlation between the transverse polarization of a fragmenting quark with flavor q and the transverse momentum distribution of the detected unpolarized hadron. It is a non-collinear fragmentation function, which allows for azimuthal hadron asymmetries that depend on the transverse hadron momentum $P_{h\perp}$. One is hence forced to account for the transverse momentum $k_\perp$ of quarks as well. This leads to the convolution $h_1^q \otimes H_1^{\perp q}$ that gives rise to a specific azimuthal modulation of the cross section. The amplitude of the modulation has been measured by the HERMES and COMPASS collaborations [9, 10]. In order to extract the transversity distribution from this signal, the Collins function should be determined through the measurement of azimuthal asymmetries in the distribution of two almost back-to-back hadrons in e^+e^- annihilation [11]. The Belle collaboration has measured this asymmetry [12, 13], making the first-ever extraction of h_1^q possible from a simultaneous analysis of $ep^\uparrow \to e'\pi X$ and $e^+e^- \to \pi\pi X$ data [14]. The transversity accessed through this process is encapsulated in the Transverse Momentum Distribution (TMD) $h_1(x, k_\perp, Q^2)$.

In spite of this breakthrough, some questions still hinder the extraction of transversity from semi-inclusive measurements. A crucial issue is the treatment of Q^2-evolution, since the measurements were performed at very different energies. The convolution $h_1^q \otimes H_1^{\perp q}$ involves the transverse momentum of quarks. Hence, its evolution should be described in the framework of the transverse-momentum-dependent factorization [15, 16]. Quantitative estimates suggest that neglecting evolution effects could lead to overestimation of transversity [17, 18]. Recent theoretical progress will allow for more accurate estimates in near future [19, 20].

It is important to extract transversity in an independent way, requiring only standard collinear factorization where the above complications are absent (see, e.g, Refs. [21, 22] and references therein). An alternative analysis of the transversity distribution has been studied through the semi-inclusive deep-inelastic production of two pions with small invariant mass,

$$\ell(l) + N(P) \to \ell(l') + H_1(P_1) + H_2(P_2) + X \quad .$$

In this case, the transversity distribution function is combined with a chiral-odd Dihadron Fragmentation Function (DiFF), denoted as $H_1^{\sphericalangle q}$ [23], which describes the correlation between the transverse polarization of the fragmenting quark with flavor q and the azimuthal orientation of the plane containing the momenta of the detected hadron pair. Contrary to the Collins mechanism, this effect survives after integration over quark transverse momenta and can be analyzed in the framework of collinear factorization. This process has been studied from different perspectives in a number of papers [24, 25, 26, 23, 27].

There are at present only two published measurements of the relevant asymmetry, one by the HERMES collaboration for the production of $\pi^+\pi^-$ pairs on transversely polarized protons [28], and the other by the COMPASS collaboration for the production of unidentified H^+H^- pairs on transversely polarized protons and deuterons [29]. Combined with the Belle data on the Artru–Collins azimuthal asymmetry [30], i.e. azimuthal orientations of the two-pion pairs in back-to-back jets in e^+e^- annihilation [31, 32], those data have made possible the first extraction of transversity in a collinear framework [33, 34], where factorization and evolution are both well understood. In other words, transversity as accessed through dihadron production is a collinear PDF $h_1(x, Q^2)$, i.e. with no transverse-momentum dependence. Since the errors on the deuteron measurements are substantial, the flavor separation remains unsatisfactory.

There seems to be no discrepancy between these two approaches, TMD and collinear. Nevertheless, this half-conclusion only concerns the kinematical ranges studied up to now. As it will be explained in this proposal, there is still a largely uncovered range in Bjorken-x, Q^2 and few data points exist. New results on the evolution of the Collins FF could change this trend [35].

As a matter of fact, transversity data are still scarce compared to the data for f_1 and g_1. For the Collins asymmetry in single-hadron production, there are about 100 points in x, including the recent neutron data from Hall A on a transversely polarized ^{3}He target [36]. At present, the total set of dihadron data is limited to about 20 points in x within the range $x \in [0.005, 0.3]$. The available COMPASS results come from data taken in the 2002-2004 run on a ^{6}LiD deuteron target, and from the 2007 run on a NH_3 proton target [29]. The collaboration are now analyzing new data collected in the 2010 run on a proton target. Related unidentified pair production in proton-proton scattering has been presented by the

PHENIX collaboration for the 2006-2008 run at mid-rapidity and center-of-mass energy $\sqrt{s} = 200$ GeV [37]. The total amount of data is an order of magnitude less than those used for the extraction of g_1 (see, e.g., Ref. [38]).

It is why we would like to propose a similar measurement of dihadron electroproduction in SIDIS off a transversely polarized target at JLab@12GeV. It has been shown, in PAC 39 (proposal PR12-12-009), that CLAS12 offers the possibility of exploring a wider kinematical range, especially in x, for dihadron production in SIDIS. Thanks to their HD ice target, which will significantly improve the determination of transversity.

Of course, an independent measurement at Hall A SoLID, which has much higher luminosity, would increase the number of data points, improving the precision of the transversity extraction in the valence region. Measurements with proton provide access to a specific combination of u and d-quark contributions in one way, requiring additional assumptions to separate them. More importantly, an independent measurement at SoLID with a ^{3}He target, for which the nuclear effects have been studied [39, 40], would provide precision measurements of a different combination of u and d-quark contributions in the valence region. It will allow to do a flavor separation of the valence transversities, leading also to a better constrained tensor charge.

We also propose to investigate a possible Sivers effect in dihadron SIDIS. The latter involves unpolarized TMD DiFFs coupled to the Sivers function, a T-odd TMD that has been, so far, accessed only in single-pion SIDIS [41, 42, 43, 44, 45] —in a TMD factorization framework as well.

2 Theoretical framework

2.1 Preamble on nuclear effects

Transversely polarized ^{3}He target offers the possibility to study single spin asymmetries of a 'free' neutron. The Helium-3 is composed of 2 protons and one neutron, but the contribution to the asymmetries from the proton is very small comparing to that from the neutron because of particular spin configuration of the target, i.e. the two protons' spin are opposite so that their contributions to the asymmetries largely are canceled out. Procedures to extract the neutron spin-dependent structure functions from ^{3}He data in inclusive DIS, taking properly into account the Fermi motion and binding effects, have been proposed and successfully applied. It has been repeated for single-hadron SIDIS [39, 40]. Fermi motion and binding effects within the Impulse Approximation, in the approach of the mentioned references, are under control. Moreover, such effects for the single-hadron SIDIS case, in the model approximations of the cited references, seem to be small at mid-x range, i.e. the region of interest here. The nuclear effects have not been studied for dihadron production. For now, we assume they are of the same order of magnitude as for the single-hadron case. The extraction of Ref. [39] relies on proton data. In that sense, the data on ^{3}He will be complementary to proton data.

The Impulse Approximation can be safely applied for pions that are detected at small angles with respect to the virtual photon direction, and with a large longitudinal fraction z. The cut in z usually comes from the selection of current fragmentation $-x_F > 0-$ for the two

pions. In dihadron's case, the distribution of both z's *w.r.t.* x_F is shown on Fig. 1.

In a SIDIS process the effect of Final State Interactions cannot be neglected a priori. This effect has been investigated in Ref. [46] including a distorted spin-dependent spectral function introduced by applying a generalized eikonal approximation, already successfully exploited for describing unpolarized SIDIS off nuclei [47]. A thorough knowledge about the distorted spin-dependent spectral function would allow one to reliably separate the effects owing to the nuclear structure from the ones involving partonic quantities. In Ref. [46], the investigation of the spin-dependent spectral function needed for describing the spectator SIDIS model has allowed to single out a kinematical region where the FSI can be minimized and a region where the FSI has a maximal effect.

The nuclear corrections related to the present proposal are under control.

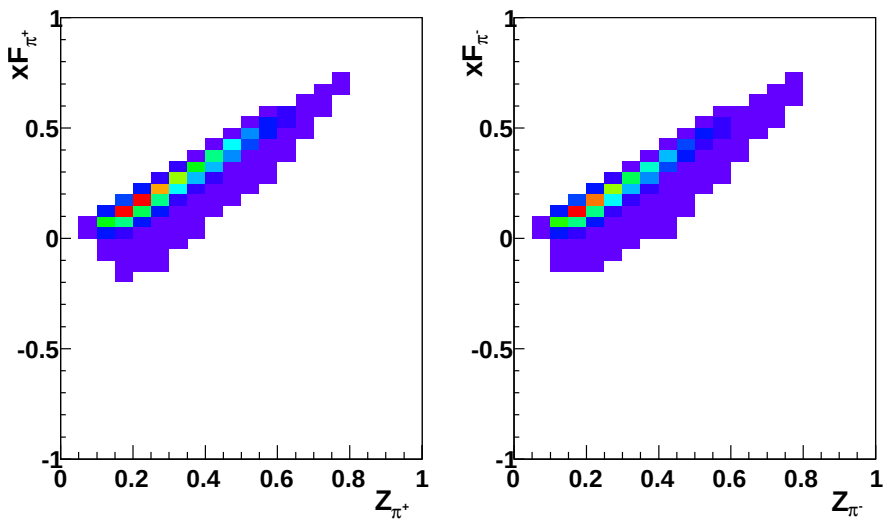

Figure 1: The individual z for each hadron against the variable x_F.

2.2 Dihadron SIDIS framework

Hence, we consider the process

$$\ell(l) + N(P) \to \ell(l') + H_1(P_1) + H_2(P_2) + X, \tag{1}$$

where ℓ denotes the beam lepton, N the neutron target, H_1 and H_2 the produced hadrons, and where four-momenta are given in parentheses. We work in the one-photon exchange approximation and neglect the lepton mass. We denote by M the mass of the nucleon and by S its polarization. The final hadrons, with mass M_1, M_2 and momenta P_1, P_2, have invariant mass M_h(which we consider much smaller than the hard scale $Q^2 = -q^2 \geq 0$ of the SIDIS process). We introduce the pair total momentum $P_h = P_1 + P_2$ and relative momentum $R = (P_1 - P_2)/2$.

As usual we define $q = l - l'$ and introduce the variables

$$x = \frac{Q^2}{2\,P\cdot q}, \qquad y = \frac{P\cdot q}{P\cdot l}, \qquad z = \frac{P\cdot P_h}{P\cdot q}, \qquad \gamma = \frac{2Mx}{Q}. \tag{2}$$

In the center-of-mass (cm) frame of the two hadrons, the emission occurs back-to-back and the key variable is the polar angle θ between the directions of the emission and the direction of P_h in the photon-nucleon center-of-mass frame.

Finally, the azimuthal angles are defined as in Fig. 2 [28].[1]

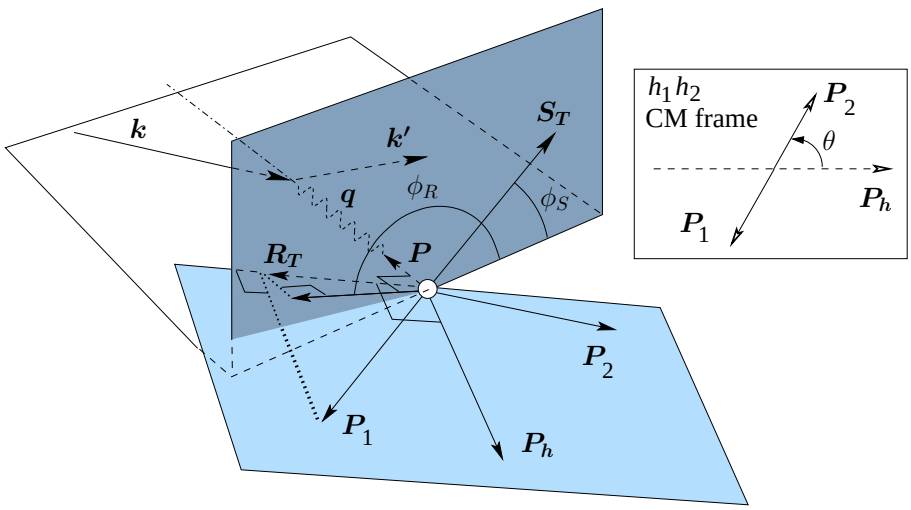

Figure 2: Definition of the azimuthal angles ϕ_R of the dihadron system and ϕ_S of the target-polarization $\boldsymbol{S}_T$, *i.e.* the component transverse to both the virtual-photon ($\boldsymbol{q}$) and target-nucleon momenta ($\boldsymbol{P}$), respectively. Both angles are evaluated in the virtual-photon–nucleon center-of-momentum frame. Here, $\boldsymbol{R}_T = \boldsymbol{R} - (\boldsymbol{R}\cdot\hat{\boldsymbol{P}}_h)\hat{\boldsymbol{P}}_h$, i.e., R_T is the component of P_1 orthogonal to P_h; up to subleading-twist corrections, it can be identified with its projection to the plane perpendicular to $\boldsymbol{q}$ that contains $\boldsymbol{S}_T$. Thus, the angle ϕ_R is the azimuthal angle of R_T about the virtual-photon direction. Explicitly, $\phi_R \equiv \frac{(\boldsymbol{q}\times\boldsymbol{k})\cdot\boldsymbol{R}_T}{|(\boldsymbol{q}\times\boldsymbol{k})\cdot\boldsymbol{R}_T|}\arccos\frac{(\boldsymbol{q}\times\boldsymbol{k})\cdot(\boldsymbol{q}\times\boldsymbol{R}_T)}{|\boldsymbol{q}\times\boldsymbol{k}||\boldsymbol{q}\times\boldsymbol{R}_T|}$ and $\phi_S \equiv \frac{(\boldsymbol{q}\times\boldsymbol{k})\cdot\boldsymbol{S}_T}{|(\boldsymbol{q}\times\boldsymbol{k})\cdot\boldsymbol{S}_T|}\arccos\frac{(\boldsymbol{q}\times\boldsymbol{k})\cdot(\boldsymbol{q}\times\boldsymbol{S}_T)}{|\boldsymbol{q}\times\boldsymbol{k}||\boldsymbol{q}\times\boldsymbol{S}_T|}$. Also included is a description of the polar angle θ, which is evaluated in the center-of-momentum frame of the pion pair.

[1] From the theoretical point of view, different definitions for the azimuthal angles may be adopted, as long as they differ by terms of order γ^2.

To leading-order, the cross section for two-particle inclusive DIS can be written as [48]

$$
\begin{aligned}
&\frac{d\sigma}{dx\,dy\,d\psi\,dz\,d\phi_R\,dM_h^2\,d\cos\theta} = \\
&\quad \frac{\alpha^2}{xy\,Q^2}\,\frac{y^2}{2\,(1-\varepsilon)}\left(1+\frac{\gamma^2}{2x}\right)\Bigg\{F_{UU,T} + \varepsilon\,F_{UU,L} + \sqrt{2\,\varepsilon(1+\varepsilon)}\,\cos\phi_R\,F_{UU}^{\cos\phi_R} \\
&\qquad + \varepsilon\cos(2\phi_R)\,F_{UU}^{\cos 2\phi_R} + \lambda_e\,\sqrt{2\,\varepsilon(1-\varepsilon)}\,\sin\phi_R\,F_{LU}^{\sin\phi_R} \\
&\qquad + S_L\left[\sqrt{2\,\varepsilon(1+\varepsilon)}\,\sin\phi_R\,F_{UL}^{\sin\phi_R} + \varepsilon\sin(2\phi_R)\,F_{UL}^{\sin 2\phi_R}\right] \\
&\qquad + S_L\lambda_e\left[\sqrt{1-\varepsilon^2}\,F_{LL} + \sqrt{2\,\varepsilon(1-\varepsilon)}\,\cos\phi_R\,F_{LL}^{\cos\phi_R}\right] \\
&\qquad + |\boldsymbol{S}_T|\Bigg[\sin(\phi_R-\phi_S)\left(F_{UT,T}^{\sin(\phi_R-\phi_S)} + \varepsilon\,F_{UT,L}^{\sin(\phi_R-\phi_S)}\right) \\
&\qquad\quad + \varepsilon\,\sin(\phi_R+\phi_S)\,F_{UT}^{\sin(\phi_R+\phi_S)} + \varepsilon\,\sin(3\phi_R-\phi_S)\,F_{UT}^{\sin(3\phi_R-\phi_S)} \\
&\qquad\quad + \sqrt{2\,\varepsilon(1+\varepsilon)}\,\sin\phi_S\,F_{UT}^{\sin\phi_S} + \sqrt{2\,\varepsilon(1+\varepsilon)}\,\sin(2\phi_R-\phi_S)\,F_{UT}^{\sin(2\phi_R-\phi_S)}\Bigg] \\
&\qquad + |\boldsymbol{S}_T|\lambda_e\Bigg[\sqrt{1-\varepsilon^2}\,\cos(\phi_R-\phi_S)\,F_{LT}^{\cos(\phi_R-\phi_S)} + \sqrt{2\,\varepsilon(1-\varepsilon)}\,\cos\phi_S\,F_{LT}^{\cos\phi_S} \\
&\qquad\quad + \sqrt{2\,\varepsilon(1-\varepsilon)}\,\cos(2\phi_R-\phi_S)\,F_{LT}^{\cos(2\phi_R-\phi_S)}\Bigg]\Bigg\},
\end{aligned}
\tag{3}
$$

where α is the fine structure constant, λ_e is the beam longitudinal polarization, and the structure functions on the r.h.s. depend on x, Q^2, z, $\cos\theta$, and M_h^2. The angle ψ is the azimuthal angle of ℓ' around the lepton beam axis with respect to an arbitrary fixed direction, which in case of a transversely polarized target we choose to be the direction of S. The corresponding relation between ψ and ϕ_S is given in Ref. [49]; in deep inelastic kinematics one has $d\psi \approx d\phi_S$. The first and second subscripts of the above structure functions indicate the respective polarization of beam and target, whereas the third subscript in $F_{UU,T}$, $F_{UU,L}$ and $F_{UT,T}^{\sin(\phi_h-\phi_S)}$, $F_{UT,L}^{\sin(\phi_h-\phi_S)}$ specifies the polarization of the virtual photon. Note that here longitudinal or transverse target polarizations refer to the photon direction. The conversion to the experimentally relevant longitudinal or transverse polarization w.r.t. the lepton beam direction is straightforward and given in [49].

The ratio ε of longitudinal and transverse photon flux in (3) is given by [48]

$$
\varepsilon = \frac{1-y-\frac{1}{4}\gamma^2y^2}{1-y+\frac{1}{2}y^2+\frac{1}{4}\gamma^2y^2}, \tag{4}
$$

so that the depolarization factors can be written as

$$\frac{y^2}{2\,(1-\varepsilon)} = \frac{1}{1+\gamma^2}\left(1-y+\tfrac{1}{2}y^2+\tfrac{1}{4}\gamma^2y^2\right) \approx \left(1-y+\tfrac{1}{2}y^2\right) \equiv A(y) \quad , \tag{5}$$

$$\frac{y^2}{2\,(1-\varepsilon)}\,\varepsilon = \frac{1}{1+\gamma^2}\left(1-y-\tfrac{1}{4}\gamma^2y^2\right) \approx (1-y) \equiv B(y) \quad , \tag{6}$$

$$\frac{y^2}{2\,(1-\varepsilon)}\sqrt{2\,\varepsilon(1+\varepsilon)} = \frac{1}{1+\gamma^2}\,(2-y)\sqrt{1-y-\tfrac{1}{4}\gamma^2y^2} \approx (2-y)\sqrt{1-y} \equiv V(y) \quad , \tag{7}$$

$$\frac{y^2}{2\,(1-\varepsilon)}\sqrt{2\,\varepsilon(1-\varepsilon)} = \frac{1}{\sqrt{1+\gamma^2}}\,y\sqrt{1-y-\tfrac{1}{4}\gamma^2y^2} \approx y\sqrt{1-y} \equiv W(y) \quad , \tag{8}$$

$$\frac{y^2}{2\,(1-\varepsilon)}\sqrt{1-\varepsilon^2} = \frac{1}{\sqrt{1+\gamma^2}}\,y\left(1-\tfrac{1}{2}y\right) \approx y\left(1-\tfrac{1}{2}y\right) \equiv C(y) \quad . \tag{9}$$

The relevant spin asymmetries can be built as ratios of structure functions. Different choices and definitions are possible. Here we try to be consistent with the past literature [28] and the Trento conventions [50].

For an unpolarized beam and a transversely polarized target, i.e. for the UT combination, one can define the following asymmetry:

$$\begin{aligned} A_{UT}^{\sin(\phi_R+\phi_S)}(x,y,z,M_h,Q) &= \frac{1}{|\boldsymbol{S}_T|}\,\frac{\frac{8}{\pi}\int d\phi_R\,d\cos\theta\,\sin(\phi_R+\phi_S)\,(d\sigma^{\uparrow}-d\sigma^{\downarrow})}{\int d\phi_R\,d\cos\theta\,(d\sigma^{\uparrow}+d\sigma^{\downarrow})} \\ &= \frac{\frac{4}{\pi}\,\varepsilon\int d\cos\theta\,F_{UT}^{\sin(\phi_R+\phi_S)}}{\int d\cos\theta\,(F_{UU,T}+\varepsilon\,F_{UU,L})} \quad . \end{aligned} \tag{10}$$

In the limit[2] of $M_h^2 \ll Q^2$, he structure functions can be written in terms of PDFs and DiFFs [52], to leading-order:

$$F_{UU,T} = \sum_q e_q^2\,x\,f_1(x)\,D_1\big(z,\cos\theta,M_h\big) \quad , \tag{11}$$

$$F_{UU}^{\cos\phi_R} = -\sum_q e_q^2\,x\frac{|\boldsymbol{R}|\sin\theta}{Q}\,\frac{1}{z}\,f_1(x)\,\widetilde{D}^{\sphericalangle}\big(z,\cos\theta,M_h\big) \quad , \tag{12}$$

$$F_{UT}^{\sin(\phi_R+\phi_S)} = \sum_q e_q^2\,x\frac{|\boldsymbol{R}|\sin\theta}{M_h}\,h_1(x)\,H_1^{\sphericalangle}\big(z,\cos\theta,M_h^2\big) \quad , \tag{13}$$

$$\begin{aligned} F_{UT}^{\sin\phi_S} = \sum_q e_q^2\,x\frac{M_h}{Q}\Bigg[h_1(x)\left(\frac{1}{z}\,\widetilde{H}\big(z,\cos\theta,M_h^2\big)+\frac{|\boldsymbol{R}|^2\sin\theta^2}{M_h^2}\,H_1^{\sphericalangle\,o\,(1)}\big(z,\cos\theta,M_h^2\big)\right) \\ -\frac{M}{M_h}\,x\,f_T(x)\,D_1\big(z,\cos\theta,M_h^2\big)\Bigg] \quad , \end{aligned} \tag{14}$$

$$F_{LT}^{\cos\phi_R} = \sum_q e_q^2\,\frac{M_h}{Q}\left[-\frac{M}{M_h}\,x\,g_T(x)\,D_1\big(z,\cos\theta,M_h^2\big)-\frac{1}{z}\,h_1(x)\,\widetilde{E}\big(z,\cos\theta,M_h^2\big)\right] \quad , \tag{15}$$

[2]For some discussion of the case $\Lambda_{\rm QCD}^2 < M_h^2 \approx Q^2$, see Ref. [51].

All other (unshown here) structure functions for transversely polarized target are zero. To be more concise, we have used the definition

$$|\boldsymbol{R}| = \frac{1}{2}\sqrt{M_h^2 - 2(M_1^2 + M_2^2) + (M_1^2 - M_2^2)^2}\ . \tag{16}$$

All the structure functions that vanish can be nonzero at order $\mathcal{O}\left(\frac{M^2}{Q^2}, \frac{M_h^2}{Q^2}\right)$. The higher-twist DiFFs are defined in Ref. [52]. In the present proposal, we focus on the leading-twist effects. Hence, the most interesting term for our purposes is the structure function containing the PDF h_1, multiplied by the interference fragmentation function $H_1^{\sphericalangle}$, occurring in the structure functions $F_{UT}^{\sin(\phi_R+\phi_S)}$ of Eq. (13). The extraction of the transversity PDF in Ref. [34] was made possible by the fact that $H_1^{\sphericalangle}$ has been recently extracted [53] from Belle measurements [30] (see the next Section).

We note that the definition of the asymmetry Eq. (10) assumes a full integration over ϕ_R and $\cos\theta$. While it is not the case due to acceptance effects, spurious modulation generated by acceptance corrections are expected to be small. A realistic coverage implies corrections in the definition of the asymmetry given by Eq. (10). Spurious mixing of modulations could appear that are related to higher-twist effects, in particular from the structure function Eq. (14) characterized by a $\sin\phi_S$ modulation, or the structure function Eq. (15) characterized by a $\cos(\phi_R)$ modulation. This issue can be studied, as it has been studied for single-pion production at SoLID, by studying the effect of including more modulations in the fit of the asymmetry. For the single-pion case, it has been done using fit/modulation with three-term (only leading-twist term) vs five-term (all terms, including higher-twist terms) —see Section 16.3 of the proposal for E12-10-006. No significant difference is expected when going from single to dihadron production. Also, higher-twist can be singled-out with a multi-dimensional binning with a good extension in Q^2 as can be seen in Figs. 24–29.

2.3 The dihadron fragmentation functions (DiFFs)

Two-hadron fragmentation functions can be decomposed into partial waves in the following way [27]:

$$D_1 \to D_{1,ss+pp} + D_{1,sp}\cos\theta + D_{1,pp}\frac{1}{4}\left(3\cos^2\theta - 1\right)\ , \tag{17}$$

$$H_1^{\sphericalangle} \to H_{1,sp}^{\sphericalangle} + H_{1,pp}^{\sphericalangle}\cos\theta\ , \tag{18}$$

where the relative partial waves of each pion pair are made evident. The notation $ss + pp$ refers to hadron pairs created with a relative $\Delta L = 0$, i.e. unpolarized ; while the sp refers the interference between pion pairs in s and p waves with a relative $\Delta L = 1$. For simplicity, we will use the notation $D_{1,ss+pp} \equiv D_1$ since no ambiguity arises in the following. The functions $\widetilde{H}$ and $\widetilde{E}$ can be expanded in the same way as D_1, and the function $\widetilde{D}^{\sphericalangle}$ in the same way as $H_1^{\sphericalangle}$. The functions on the r.h.s. depend on z and M_h. It may be useful to note that a symmetrization $f(\theta) + f(\pi - \theta)$ gets rid of all the $\cos\theta$ terms [28]. In general,

those terms will vanish even if the θ acceptance is not complete but still symmetric about $\theta = \pi/2$.

A thorough study of the cross section with a partial-wave analysis has been recently presented in Ref. [54], with a different notation compared to the one adopted here.

We now make a flavor analysis of the structure functions. The analysis will be different depending on the kind of target and final-state hadrons. We will consider here only neutron targets with $\pi^+\pi^-$ final-state pairs. Isospin symmetry and charge conjugation suggest the relations [33]

$$D_1^{u\to\pi^+\pi^-} = D_1^{\bar{u}\to\pi^+\pi^-} \ ,$$
$$D_1^{d\to\pi^+\pi^-} = D_1^{\bar{d}\to\pi^+\pi^-} \ , \tag{19}$$
$$D_1^{s\to\pi^+\pi^-} = D_1^{\bar{s}\to\pi^+\pi^-} \ ,$$
$$D_1^{c\to\pi^+\pi^-} = D_1^{\bar{c}\to\pi^+\pi^-} \ , \tag{20}$$
$$H_1^{\sphericalangle u\to\pi^+\pi^-} = -H_1^{\sphericalangle d\to\pi^+\pi^-} = -H_1^{\sphericalangle \bar{u}\to\pi^+\pi^-} = H_1^{\sphericalangle \bar{d}\to\pi^+\pi^-} \ , \tag{21}$$
$$H_1^{\sphericalangle s\to\pi^+\pi^-} = -H_1^{\sphericalangle \bar{s}\to\pi^+\pi^-} = H_1^{\sphericalangle c\to\pi^+\pi^-} = -H_1^{\sphericalangle \bar{c}\to\pi^+\pi^-} = 0 \ . \tag{22}$$

In this proposal, for $\pi^+\pi^-$, we consider that

$$D_1^{u\to\pi^+\pi^-} = D_1^{d\to\pi^+\pi^-} \quad , \tag{23}$$

meaning that we can safely neglect that effect from the K_S resonance in a first approximation. In practice, there are only three independent D_1 functions and one $H_1^{\sphericalangle}$ function.

$K^+\pi^-$ pairs could be included in the future. In absence of e^+e^- information on DiFF for such pairs, more approximations would be necessary.

Before the Belle measurement of the angular distribution of two pion pairs in e^+e^- annihilation [30], the only estimates of DiFFs were based on model calculations [55, 23, 56]. The unpolarized D_1 was tuned to Monte Carlo event generators [56] and the polarized $H_{1,sp}^{\sphericalangle}$ compared to HERMES asymmetry data [57]. Recently the unpolarized and chiral-odd DiFFs have been calculated in the NJL-jet model, respectively, in Ref. [58, 59] and Ref. [60].

The first analysis [30] of the so-called Artru–Collins asymmetry [61] by the Belle collaboration made possible a direct extraction of $H_{1,sp}^{\sphericalangle}$ for the production of $\pi^+\pi^-$.

In the absence of a measurement of the unpolarized cross section for dihadron production in e^+e^- annihilation (planned at Belle in the near future), D_1 was parametrized to reproduce the two-hadron yields of the PYTHIA event generator, which is known to give a good description of data. Four main decay channels were considered for $\pi^+\pi^-$: (i) ρ resonance decaying into the two pions, (ii) ω resonance decaying into the two pions, plus the fragmentation into a ω resonance decaying into $\pi^+\pi^-\pi^0$ with π^0 unobserved, (iii) K_S^0 resonance decaying into $(\pi^+\pi^-)$ (whose effect on Eq. (23) is neglected here), (iv) the continuum (*i.e.* the fragmentation into an "incoherent" $\pi^+\pi^-$ pair). Combining the parametrization of the unpolarized functions D_1 with the fit of the azimuthal asymmetry presented in Ref. [30], it was possible to extract the DiFF $H_{1,sp}^{\sphericalangle}$ [53].

In Fig. 3, we show the ratio

$$R(z, M_{\pi\pi}) = \frac{|\boldsymbol{R}|}{M_{\pi\pi}} \frac{H_{1,sp}^{\sphericalangle u}(z, M_{\pi\pi}; Q_0^2)}{D_1^u(z, M_{\pi\pi}; Q_0^2)} \ , \tag{24}$$

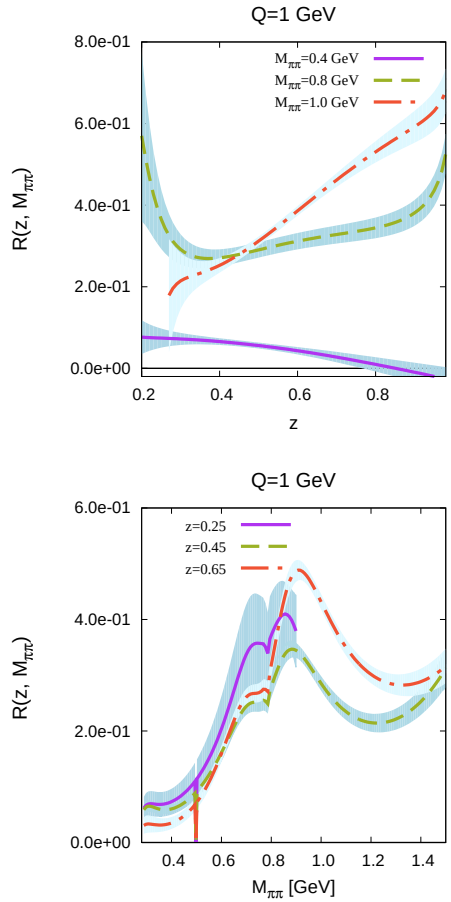

Figure 3: The ratio $R(z,M_{\pi^+\pi^-})$ of Eq. (24) as a function of z and $M_{\pi\pi}$, (left) and (right), respectively. The error bars come from the calculation of error propagation from the fit.

summed over all channels, at the hadronic scale $Q_0^2 = 1$ GeV^2. The errors are estimated through the propagation from the fit.

Evolution effects affect both D_1 and $H_1^{\sphericalangle}$ separately, but the Q^2-dependence is found to cancel to a large extent when taking the ratio $H_1^{\sphericalangle}/D_1$ in the asymmetry [57].

For the purposes of extracting the transversity distribution, the most relevant quantities are the integrals

$$\begin{aligned} n_q(Q^2) &= \int dz\, dM_{\pi\pi}\, D_1^q(z, M_{\pi\pi}; Q^2) \\ n_q^{\uparrow}(Q^2) &= \int dz\, dM_{\pi\pi}\, \frac{|\boldsymbol{R}|}{M_{\pi\pi}}\, H_{1,sp}^{\sphericalangle q}(z, M_{\pi\pi}; Q^2)\ , \end{aligned} \tag{25}$$

where the lower and upper limits are set by the limits of the bins.

2.4 The transversity distribution function

A comprehensive review of the properties of the transversity distribution function can be found in Ref. [6]. Transversity h_1, as leading-twist collinear PDF, enjoys the same status as f_1 and g_1 [1, 62]. The distribution of transversely polarized quarks $q^\uparrow$ in a transversely polarized nucleon $p^\uparrow$ (integrated over transverse momentum) can be written as

$$f_{q^\uparrow/p^\uparrow}(x) = f_1^q(x) + \boldsymbol{S} \cdot \boldsymbol{S}_q \, h_1^q(x) \quad , \tag{26}$$

in which $\boldsymbol{S}$ is the nucleon spin and $\boldsymbol{S}_q$ the quark spin. Therefore, transversity can be interpreted as the difference between the probability of finding a parton (with flavor q and momentum fraction x) with transverse spin parallel and anti-parallel to that of the transversely polarized nucleon.

In a non-relativistic framework $h_1 = g_1$, but relativistically h_1 and g_1 are different. Therefore any difference between helicity and transversity PDFs is related to the relativistic nature of parton dynamics inside hadrons.

An important difference between h_1 and g_1 is that in spin-$\frac{1}{2}$ hadrons there is no gluonic function analogous to transversity. The most important consequence is that h_1^q for a quark with flavor q does not mix with gluons in its evolution and it behaves as a non-singlet quantity; this has been verified up to NLO, where chiral-odd evolution kernels have been studied so far [63, 64, 65].

There are three complementary extractions of the transversity distributions: the TMD parametrization (also known as Torino fit) [66, 67], the collinear extraction (also known as Pavia fit) [33, 34] and the GPD approach (GGL) [68]. The former is based on the TMD framework in which the chiral-odd partner of $h_1(x, k_\perp)$ is the Collins fragmentation function ; the second is based on a collinear framework, involving the chiral-odd dihadron fragmentation function, i.e. $H_1^{\sphericalangle}$, and is of interest here. The GPD approach relates the DVCS data to the transversity as the forward limit of the chiral-odd GPD H_T.

One of the main differences lie in that the collinear extraction does not require the use of a fitting functional form: it is a point-by-point extraction. However, for practical reasons, a statistical study of the transversity PDF has been performed as well. So far, both approaches has found compatible results in the range in x where data exist. It is important to notice that the parameterizations are biased by the choice of the fitting functional form. The behavior of the best-fit parametrization is largely unconstrained outside the range of data, leading to confusing results at low and large-x values. This is nicely illustrated by the collinear transversity collaboration, on Fig. 4, where 2 different functional forms, with a equally good $\chi^2/d.o.f.$, have been used.

Ref. [6] lists various classes of models for the transversity distribution including bag-like models, e.g. [2]; chiral quark soliton models, e.g. [69]; light-cone models, e.g. [70]; and diquark spectator models, e.g. [71]. A comparison of the models results shows that, at low momentum scales, h_1 is not so different from g_1, at least for the dominant u sector. It would therefore be interesting to explore this more deeply by gathering more experimental data.

In Fig. 5, we show several model calculations of transversity compared to the old version of the TMD parametrization of Ref. [66].

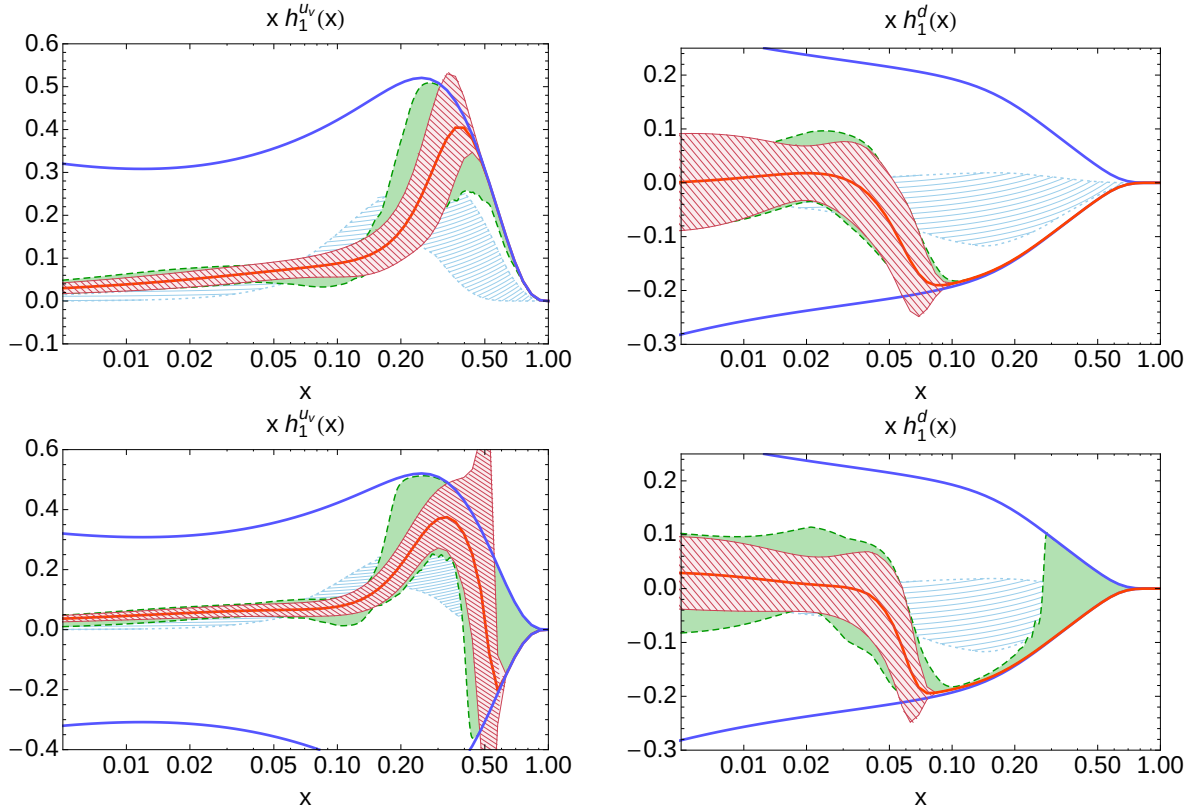

Figure 4: Fit of valence collinear transversities at $Q^2 = 2.4\text{GeV}^2$. For u and d distributions, respectively, left and right columns. The two upper plots correspond to the fits using a flexible parametrization, while the two lower plots correspond to a fit using an extra-flexible parametrization, see Ref. [34]. The red bands represent the standard fit within 1σ errors, while the green bands stand for a 1σ Monte Carlo based analysis ($n \times 68\%$ fit of n data replica at 1σ). The light blue bands correspond the the Torino fit [67] and the full blue curves to the Soffer bound.

Two important remarks are in order: first, no data exist for $x > 0.4$; secondly, the *sign* of the up quark distribution cannot be determined from experimental measurements.

A quantity of high interest is the tensor charge. The tensor charge of the nucleon is defined as the sum of the Mellin moments

$$\delta_T q(Q^2) = \int dx \left[h_1^q(x, Q^2) - h_1^{\bar{q}}(x, Q^2) \right] \quad . \tag{27}$$

Contrary to the axial charge — which is related to $g_1^q(x, Q^2)$ — it has a non-vanishing anomalous dimension and therefore evolves with the hard scale Q^2 [62]. It has been calculated on the lattice [5] and in various models [78, 76, 81, 82, 83], and it turns out not to be small. While the axial charge is a charge-even operator, from Eq. (27) it is evident that the tensor charge is odd under charge conjugation and, therefore, it does not receive contributions from $q\bar{q}$ pairs in the sea and is dominated by valence contributions. This feature, and the typical

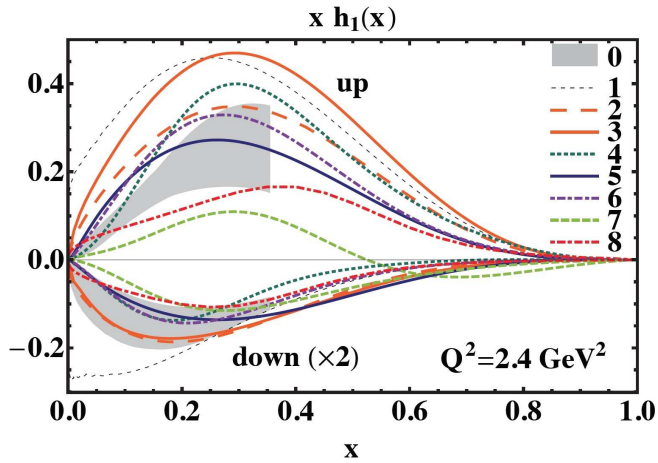

Figure 5: Model calculations of the transversity distribution function compared to available parametrization: (0–shaded band) extraction from ref. [66]; (1) saturated Soffer bound [72, 73]; (2) $h_1 = g_1$ [74]; (3-4) chiral quark-soliton models [75, 76]; (5) light-cone constituent quark model [77]; (6-7) quark-diquark models [78, 79], (8) quantum statistical approach [80].

non-singlet evolution, suggest that transversity is one of the best tools to explore the valence part of the partonic content of the nucleon. In Fig. 6, we show some estimates of the tensor charge for up and down quarks separately, together with the combined results of old TMD transversity extraction [66] (red triangles). While in Fig. 8, we show $\delta_T u$ against $\delta_T d$ for the three extractions as well as for lattice results.

Recent progress on the extraction of transversity has been achieved in the last years. Both the TMD and collinear transversities groups have updated their fits. On Fig. 7, we illustrate the importance of the data range on the determination of the tensor charge. On the left hand side, we show the tensor charge for the u quark integrated only over the range of the available data. All functional forms, though very different, lead to a single compatible value. On the other hand, when integrating over the whole support in x, we extrapolate the results of the fit outside the range where transversity is known. The results are illustrated on the right hand side of Fig. 7: there is no unique tensor charge estimate. We also show the resulting tensor charge for the TMD transversity parametrization. The error band on the tensor charges calculated from that parametrization are certainly underestimated, since they do not take into account the errors due to the extrapolation outside the x-range where data are presently available. Similar conclusions hold for the d transversity.

The only first principle based property on the transversity distribution is the Soffer inequality. Because a probability must be positive, we get the important Soffer inequality [72],

$$2|h_1^q(x, Q^2)| \leq f_1^q(x, Q^2) + g_1^q(x, Q^2) \ , \tag{28}$$

which is true at all values of Q^2 [89, 65]. An analogous relation holds for antiquark distributions. All of the models, including the lattice predictions, find a positive tensor charge for the u-quark and a negative one for the d-quark. There are no data so far to verify this inequality.

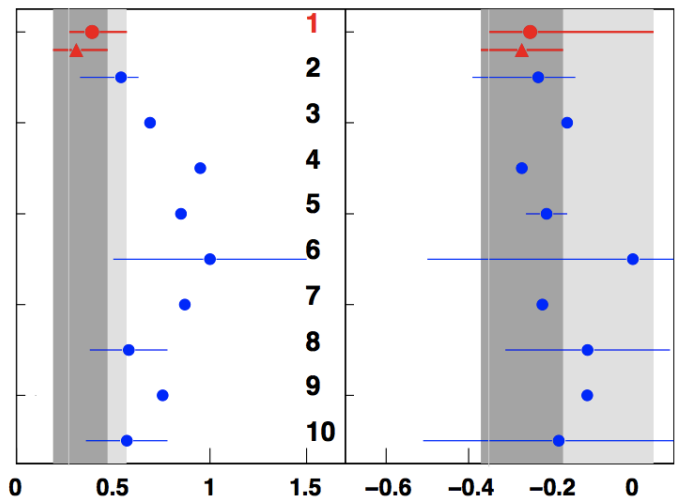

Figure 6: The tensor charge $\delta q \equiv \int_0^1 dx\,[\Delta_T q(x) - \Delta_T \bar{q}(x)]$ for u (left) and d (right) quarks, computed using the transversity distributions from TMD collaboration [67] (fitting A_{12}: top solid red circles, fitting A_0: solid red triangles). The gray areas correspond to the statistical uncertainty bands in that extraction. These results are compared with the 2009 TMD extraction [66] (number (2)) and with the results of the model calculations in (3) the quark-diquark model [78],(4) the chiral quark-soliton model [76], (5) lattice QCD [84], (6) sum rules [81], (7) a constituent quark model [82], (8) spin-flavour SU(6) symmetry [83] and (9) Dyson-Schwinger with dressed constituents [85]. A recent calculation in Dyson-Schwinger including axial-vector diquarks with contact interaction gives $\delta u \sim 0.3$ and $\delta d \sim -0.2$ [86]. The number (10) corresponds to the standard rigid version of the fit via DiFF [34], see Fig. 7 for comparison of the 2 fits' results.

In this proposal, we have considered three estimates for $h_1(x)$: the Light-Cone Constituent Quark Model prediction(LCCQM) [82], the diquark spectator model prediction [79], the TMD extraction of Ref. [66] as well as the very new collinear extaction of Ref. [34]. They are all shown in Fig. 9.

2.4.1 Single Spin Asymmetries: predictions for h_1

Using the expressions of the structure functions Eqs. (11)–(15), dropping corrections of order $\mathcal{O}(M^2/Q^2)$, and inserting the partial-wave expansion of the fragmentation functions in Eqs. (17)–(18), we can rewrite the asymmetry in Eq. (10), for a neutron target, as

$$A_{UT,n}^{\sin(\phi_R+\phi_S)}(x,y,z,M_{\pi\pi},Q) = -\frac{B(y)}{A(y)}\frac{|\boldsymbol{R}|}{M_{\pi\pi}}\frac{e_u^2\, h_1^{d-\bar{d}}(x)\, H_{1,sp}^{\sphericalangle,u}(z,M_{\pi\pi}) + e_d^2\, h_1^{u-\bar{u}}(x)\, H_{1,sp}^{\sphericalangle,d}(z,M_{\pi\pi})}{e_d^2\, f_1^{u+\bar{u}}(x)\, D_1^d(z,M_{\pi\pi}) + e_u^2\, f_1^{d+\bar{d}}(x)\, D_1^u(z,M_{\pi\pi}) + e_s^2\, f_1^{s+\bar{s}}(x)\, D_1^s(z,M_{\pi\pi})} \tag{29}$$

For the specific case of the $\pi^+\pi^-$ final state, we can introduce into the flavor sum the

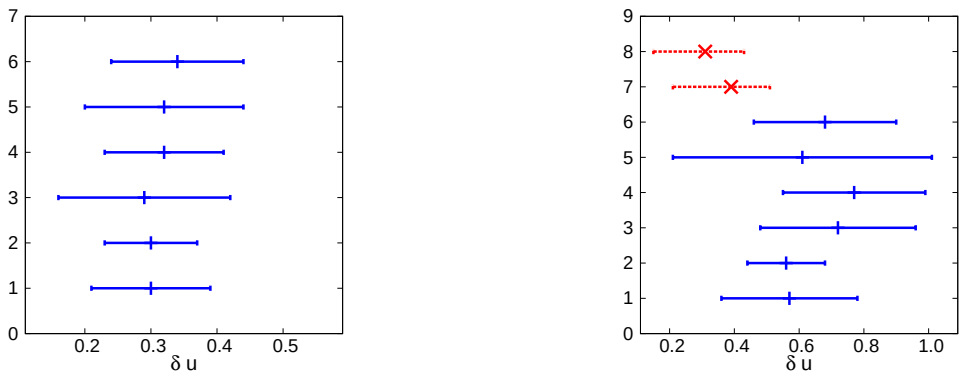

Figure 7: Left hand side: tensor charge integrated over data range for the u-quark. Right hand side: tensor charge integrated on the theoretical support $x \in [0, 1]$. Respectively for, from 1 to 8, standard rigid, Monte Carlo rigid, standard flexible, Monte Carlo flexible, standard extra-flexible, Monte Carlo extra-flexible of the collinear fit [34] and the fit for A_0 and A_{12} asymmetries at Belle combined with single-hadron SIDIS of the TMD fit collaboration [67].

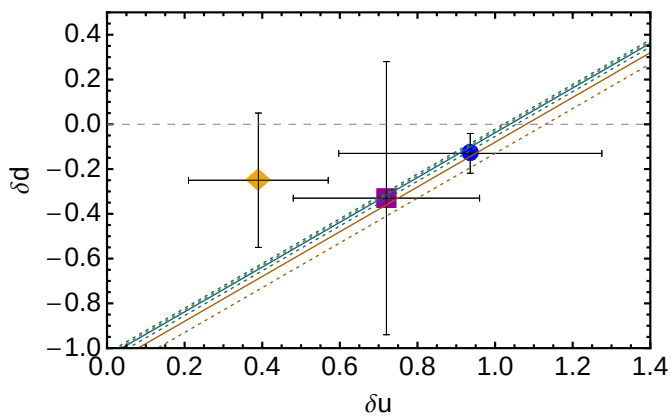

Figure 8: The tensor charge δu vs. δd, computed using the transversity distributions from TMD collaboration [67] (standard) (yellow diamond). The blue circle comes from the chiral-odd GPD H_T sum rule, with the GPD fits of Ref. [68]. The purple square corresponds to the standard flexible version of the fit via DiFF [34], see Fig. 7 for comparison of the 2 fits' results. The cyan curve corresponds to the lattice result from Ref. [87] ; the brown curve to Ref. [88].

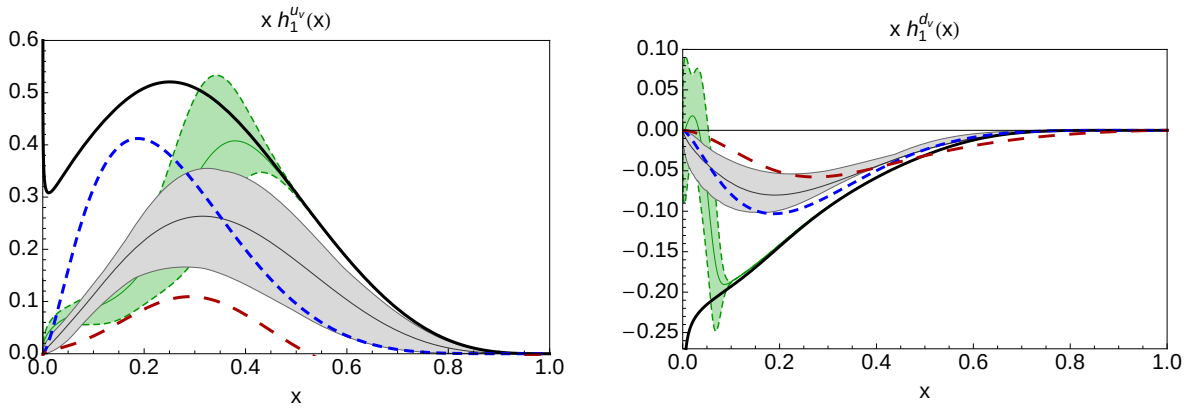

Figure 9: Estimates of $h_1(x)$ used in the present proposal for predictions, all evolved to 2.5 GeV^2. The blue short-dashed curve represents the LCCQM of Ref. [82], and the red long-dashed curve, the spectator model of Ref. [79]. The grey band is the extraction of the TMD transversities Ref. [66]. The green band represent the flexible parametrization of the collinear valence transversities of Ref. [34]. The black curve is the Soffer bound evaluated with the LO MSTW08 unpolarized PDFs [90] and the LO DSS05 polarized PDFs [91].

constraints of Eqs. (19)–(22), and we get

$$A_{UT,n}^{\sin(\phi_R+\phi_S)}(x,y,z,M_{\pi\pi},Q) = -\frac{B(y)}{A(y)}\frac{|\boldsymbol{R}|}{M_{\pi\pi}}\frac{H_{1,sp}^{\sphericalangle,u}(z,M_{\pi\pi})\left[4\,h_1^{d-\bar{d}}(x)-\,h_1^{u-\bar{u}}(x)\right]}{D_1^u(z,M_{\pi\pi})\left[f_1^{u+\bar{u}}(x)\,+4\,f_1^{d+\bar{d}}(x)\right]+D_1^s(z,M_{\pi\pi})\,f_1^{s+\bar{s}}(x)}\quad, \tag{30}$$

where we adopt the compact notation $f_1^{q\pm\bar{q}}(x) = f_1^q(x) \pm f_1^{\bar{q}}(x)$, likewise for h_1. We neglected the contribution from charm quarks.

The data on neutron target could be combined, in the future, with proton target data, like the one proposed for single-hadron at SoLID (E12-11-108), or combined with Dihadron Production in SIDIS with Transversely Polarized Proton Target at CLAS12 (PR12-12-009). Once data available for both neutron and proton, we could use Eq. (30) and the equivalent for the proton, i.e.

$$A_{UT,p}^{\sin(\phi_R+\phi_S)}(x,y,z,M_{\pi\pi},Q) = -\frac{B(y)}{A(y)}\frac{|\boldsymbol{R}|}{M_{\pi\pi}}\frac{H_{1,sp}^{\sphericalangle,u}(z,M_{\pi\pi})\left[4h_1^{u-\bar{u}}(x)-h_1^{d-\bar{d}}(x)\right]}{D_1^u(z,M_{\pi\pi})\left[4f_1^{u+\bar{u}}(x)+f_1^{d+\bar{d}}(x)\right]+D_1^s(z,M_{\pi\pi})\,f_1^{s+\bar{s}}(x)}\quad, \tag{31}$$

to extract the u_v and the d_v flavors separately.

All the unpolarized DiFFs have been studied in Ref. [53], however, for sake of **simplicity of the expressions here**, we can use the approximation $D_1^s = N_s D_1^u$. Turning to the

notation of Eq. (25), with $0 \leq N_s \leq 1$, we find

$$
\begin{aligned}
h_1^{u_v}(x) = & \frac{16}{15}\frac{n_u}{n_u^{\uparrow}} \left(\frac{A_{UT,n}}{4} \left(f_1^{u+\bar{u}}(x) + 4 f_1^{d+\bar{d}}(x) + N_s f_1^{s+\bar{s}}(x) \right) \right. \\
& \left. + A_{UT,p} \left[4 f_1^{u+\bar{u}}(x) + f_1^{d+\bar{d}}(x) + N_s\, f_1^{s+\bar{s}}(x) \right] \right) \quad , \\
h_1^{d_v}(x) = & \frac{16}{15}\frac{n_u}{n_u^{\uparrow}} \left(A_{UT,n} \left(f_1^{u+\bar{u}}(x) + 4 f_1^{d+\bar{d}}(x) + N_s f_1^{s+\bar{s}}(x) \right) \right. \\
& \left. + \frac{A_{UT,p}}{4} \left[4 f_1^{u+\bar{u}}(x) + f_1^{d+\bar{d}}(x) + N_s\, f_1^{s+\bar{s}}(x) \right] \right) \quad . \qquad (32)
\end{aligned}
$$

In that sense, the present proposal is complementary to the CLAS12 PR12-12-009 proposal on proton target.

We can now make the predictions for the asymmetries. The theoretical predictions do include the kinematical factors such as the depolarization factor. The binning chosen for the predictions on a neutron target is given in Table 1. The coverage in x is similar to what proposed at CLAS12 (PR12-12-009) and is a strong point of this proposal, as it will lead to more precision on the behavior of the transversity PDF in the large x region.

In the collinear framework, which is of interest here, the dependence on the momentum fraction x can be factorized from the $(z, M_{\pi^+\pi^-})$ dependence for each flavor, but z and $M_{\pi\pi}$ in general do not factorize. Their behavior has been studied in Refs. [56, 53] from the Belle data, which range of validity in invariant mass is $2m_\pi < M_h < 1.29$ GeV. Consequently, the dependence on $(z,\, M_{\pi\pi})$ is essentially determined by the DiFFs, while the dependence on x comes only from the PDF. The error due to the uncertainty on the DiFFs is estimated to be of about 8% for the ratio $H_1^{\sphericalangle}(\langle z\rangle_i, \langle M_{\pi\pi}\rangle_i)/D_1(\langle z\rangle_i, \langle M_{\pi\pi}\rangle_i)$. To this error should be added to the theoretical error coming from the models or the errors from the extraction of the transversities.

In Fig. 10, we show the predictions for $A_{UT,n}^{\sin(\phi_R+\phi_S)}$ from Eq. (30) at $Q^2 = 2.5$ GeV^2. When plotting the asymmetry as a function of z, it is understood that the **average values** for the corresponding bin have been used for the other 2 variables and similarly for the other two combinations.[3] The red points correspond to results obtained when using the x-dependence of the Torino parametrization for the transversity [66] ; the green points using collinear valence transversities of Ref. [34]. The blue points are produced when using the PDFs from the Light-Cone Constituent Quark Model (LCCQM) of Ref. [77], evolved at LO to 2.5 GeV^2. Since this model assumes $SU(6)$ symmetry for the proton state, in this case the asymmetry in Eq. (30) becomes

$$
A_{UT,n}^{\sin(\phi_R+\phi_S)}(x, y, z, M_{\pi\pi}, Q) = -\frac{B(y)}{A(y)} \frac{|\boldsymbol{R}|}{M_{\pi\pi}} \frac{(-4-4)/4\, h_1^u(x)\, H_{1,sp}^{\sphericalangle,u}(z, M_{\pi\pi})}{(2+4)/2\, f_1^u(x)\, D_1^u(z, M_{\pi\pi})} \quad . \qquad (33)
$$

The black points refer to the results from the spectator diquark model of Ref. [79], again evolved at LO to 2.5 GeV^2. In this model, there is no specific flavor symmetry [71] and the

[3] The integrated average differs from the bin average value only for bumpy distributions, *e.g.* the $m_{\pi\pi}$ behavior. It is a source of error as well.

$M_{\pi\pi}$(GeV) for 8.8 GeV	$M_{\pi\pi}$(GeV) for 11 GeV
0.323	0.326
0.412	0.413
0.495	0.496
0.582	0.583
0.696	0.696
0.799	0.803
0.974	1.014

Q^2 (GeV^2) for 8.8 GeV	Q^2 (GeV^2) for 11 GeV
1.089	1.097
1.312	1.318
1.594	1.607
2.015	2.087
3.111	3.415

z for 8.8 GeV	z for 11 GeV
0.369	0.360
0.451	0.449
0.531	0.531
0.616	0.615
0.717	0.714
0.811	0.818

x for 8.8 GeV	x for 11 GeV
0.	0.061
0.077	0.071
0.086	0.085
0.100	0.100
0.119	0.119
0.143	0.144
0.177	0.177
0.235	0.240
0.353	0.365

Table 1: Binning in $z, M_{\pi\pi}$ and x used in Fig. 10 for the predictions for the SSA asymmetry on neutron target (^{3}He) as well as the average value for Q^2. Left columns: 8.8 GeV polarized electron beam binning ; right columns: 11 GeV polarized electron beam binning.

asymmetry becomes

$$A_{UT,n}^{\sin(\phi_R+\phi_S)}(x,y,z,M_{\pi\pi},Q) = -\frac{B(y)}{A(y)}\frac{|\boldsymbol{R}|}{M_{\pi\pi}}\frac{H_{1,sp}^{\sphericalangle,u}(z,M_{\pi\pi})\left(4h_1^d(x)-h_1^u(x)\right)}{D_1^u(z,M_{\pi\pi})\left(4f_1^d(x)+f_1^u(x)\right)} \quad . \tag{34}$$

The $\sin(\phi_R+\phi_S)\sin\theta$ asymmetry has already been studied at HERMES for $\pi^+\pi^-$ pairs and COMPASS for unidentified pairs, [4] in different kinematics and on different targets. This made it possible to extract the relevant combinations of the u_v and d_v transversity distributions, namely $xh_1^{u_v}-xh_1^{d_v}/4$ for a transversely polarized proton target, and $xh_1^{u_v}+xh_1^{d_v}$ for a transversely polarized deuteron target. In Fig. 11, we show the results from Eq. (31) for the proton target [93, 34]. In Fig. 12, we refer to a deuteron target (proton plus neutron), described in Ref. [34]. In both cases, the effects of QCD evolution have been properly taken into account at LO in $n_u/n_u^{\uparrow}$ and in the unpolarized PDFs, including the dependence $Q^2(x)$ of the hard scale on each different experimental x bin. It can be appreciated that the error on the deuteron combination is still substantial. More precise data for the neutron distribution would greatly improve the separation in flavors as well as the range of validity of the fits.

2.5 The Sivers function

Single-hadron SIDIS processes with the detection in the final state of a produced hadron h in coincidence with the scattered electron e', is one of the proposed processes to access the

[4] Results for identified pairs have been recently presented at the DIS2013 conference.

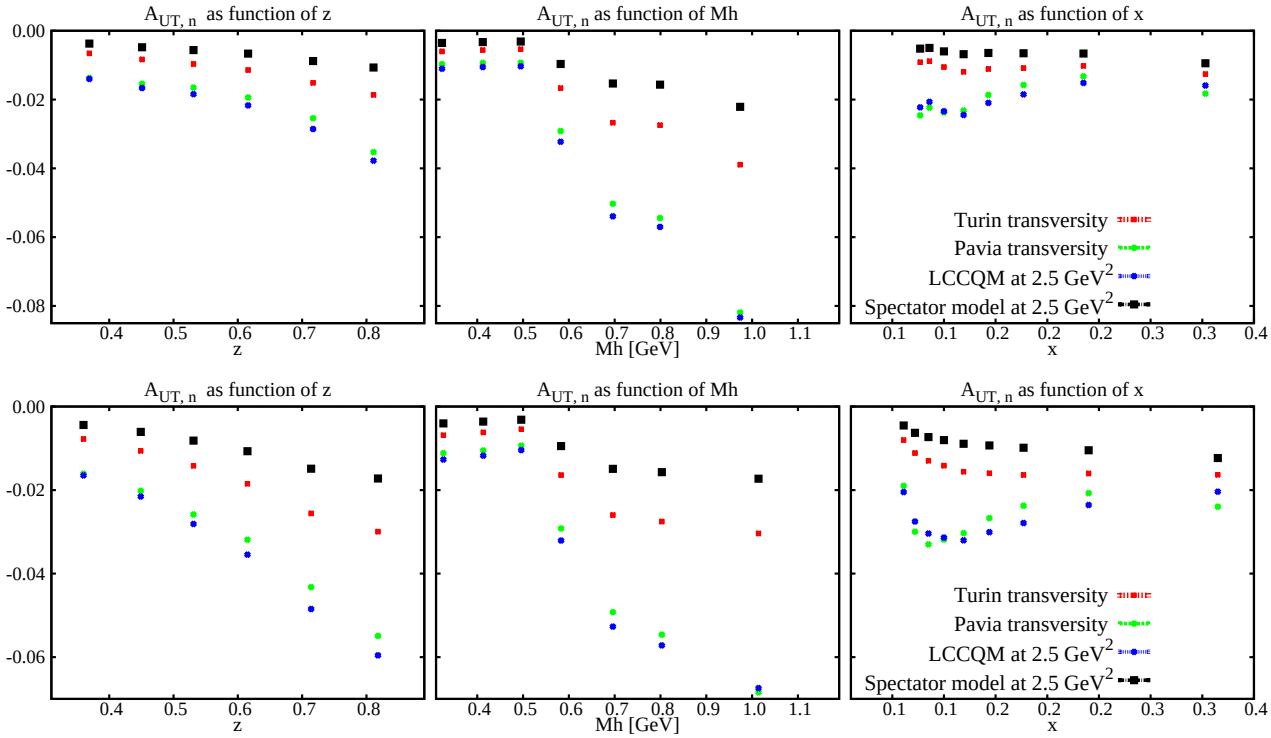

Figure 10: Predictions for the asymmetry in (z, $M_{\pi^+\pi^-}$, x). The (z,$M_{\pi^+\pi^-}$)-dependence is deduced from the extracted DiFF. The red points are deduced from the x -dependence of the TMD transversity [66] together with the MSTW08 unpolarized PDFs and the green points the collinear valence transversities [34]. The bluepoints from the Light Cone Constituent Quark Model of Ref. [82] and the black points from the spectator model of Ref. [92]. Upper panel: for an 8.8 GeV polarized electron beam, lower panel: for an 11 GeV polarized electron beam.

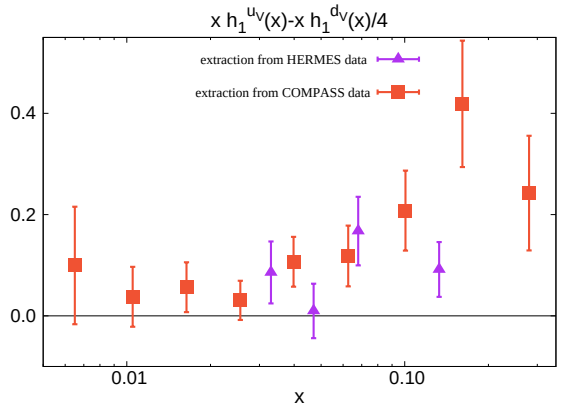

Figure 11: Transversity for the combination $h_1^{u_v} - 1/4 h_1^{d_v}$ extracted via DiFFs [93, 34], using the COMPASS data for proton (2007) (red squares) and HERMES data for proton (purple triangles).

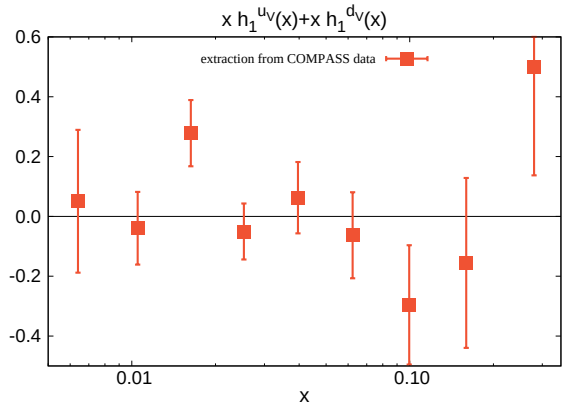

Figure 12: Transversity for the combination $h_1^{u_v} + h_1^{d_v}$ extracted via DiFFs [34], using the COMPASS data for deuteron (2002-2004) (red Squares).

parton distributions of transversely polarized hadrons. For several years it has been known that SIDIS off a transversely polarized target shows azimuthal asymmetries, the so called "single spin asymmetries" (SSAs) [94]. As a matter of fact, it is predicted that the number of produced hadrons in a given direction or in the opposite one, with respect to the reaction plane, depends on the orientation of the transverse spin of a polarized target with respect to the direction of the unpolarized beam. It can be shown that the SSA in SIDIS off transverse polarized targets is essentially due to two different physical mechanisms, whose contributions can be technically distinguished [95, 96, 97, 48]. One of them is the Collins mechanism, due to parton final state interactions in the production of a hadron by a transversely polarized quark [94], and will not be discussed here. The other is the Sivers mechanism [98], producing a term in the SSA which is given by the product of the unpolarized fragmentation function with the Sivers function, describing the number density of unpolarized quarks in a transversely polarized target. The Sivers function is a Transverse Momentum Dependent (TMD) PDF; it is a time-reversal odd object and for this reason, for several years, it was believed to vanish due to time reversal invariance. However, this argument was invalidated by a calculation in a spectator model [99], following the observation of the existence of leading-twist Final State Interactions (FSI) [100]. The current wisdom is that a non-vanishing Sivers function is generated by the gauge link in the definition of TMD parton distributions [101, 102, 103], whose contribution does not vanish in the light-cone gauge, as happens for the standard PD functions. For the same reason it is difficult to relate the Sivers Function to the target helicity-flip, impact parameter dependent, generalized parton distribution (GPD) E. Although simple relations between the two quantities are found in models [104], a clear model independent formal relation is still need to be proven, as shown in Ref. [105].

The Sivers function has been calculated in various models and extracted from single-pion SIDIS by different collaborations [41, 42, 43, 44, 45] —in a TMD factorization framework. The most recent extraction of the Sivers PDF of Ref. [43, 18] are from SIDIS measurements at HERMES and COMPASS experiments. The plots in Fig. 13 show their results for the extracted first moment of valence Sivers PDFs for u and d quark, exhibiting significant

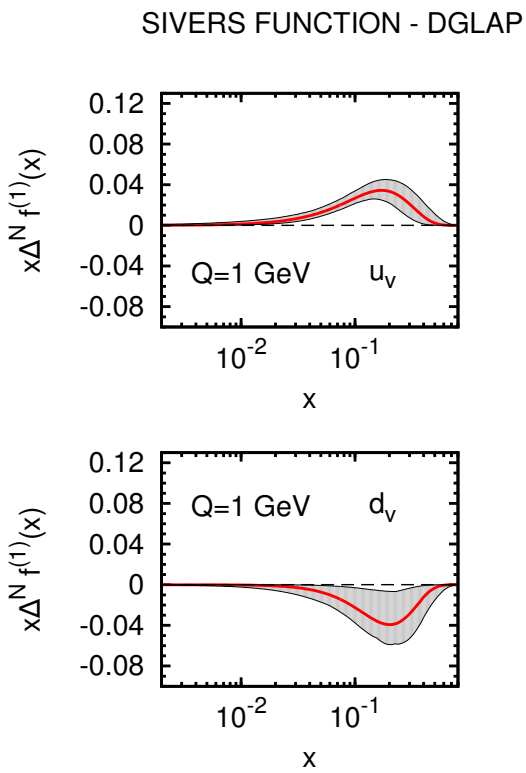

Figure 13: First moment of the Sivers function —considering "DGLAP"-like evolution— from Ref. [18].

uncertainties. Moreover, several model assumptions in these extractions can introduce also significant systematic errors.

The Sivers mechanism is particularily important for proofss on the "universality" of Distribution Functions, as it is known that its sign is process dependent.

2.5.1 Single Spin Asymmetries: predictions for the Sivers effect

We still consider the process Eq. (1) and the same kinematics.

Recently, a new approach [106, 107] has been proposed for accessing Sivers PDF in dihadron SIDIS. The terms in the fully differential cross section for two hadron production in SIDIS relevant to the Sivers effect [23, 27] are

$$d^9\sigma_{UU}^{\text{constant term}} = \sum_a \frac{\alpha^2 e_a^2}{2\pi Q^2 y}\, A(y)\, \mathcal{I}\left[f_1\, D_1\right] \quad , \tag{35}$$

$$d^9\sigma_{UT}^{\phi_h-\phi_S} = \sum_a \frac{\alpha^2 e_a^2}{2\pi Q^2 y}\, |\vec{S}_T|\, A(y) \left\{ \sin(\phi_h-\phi_S)\, \mathcal{I}\left[\frac{\vec{p}_T\cdot\hat{P}_{h\perp}}{M}\, f_{1T}^{\perp}\, D_1\right] + \cos(\phi_h-\phi_S)\, \mathcal{I}\left[\frac{\hat{P}_{h\perp}\wedge\vec{p}_T}{M}\, f_{1T}^{\perp}\, D_1\right]\right\}, \tag{36}$$

where we introduced the shorthand notation

$$\mathcal{I}[f] \equiv \int d\vec{p}_T d\vec{k}_T \, \delta(\vec{p}_T - \vec{P}_{h\perp}/z - \vec{k}_T) \, [f] \, . \tag{37}$$

Since the Sivers function is thought to depend on p_T^2 — with $\mathbf{p}_T$ the intrinisic transverse momentum of the quarks, this effect vanishes when integrated over the transverse momentum [27]. However, the new approach of Refs. [106, 107] suggests that such an effect is actually non-vanishing and even sizable. The cross sections of Eqs. (35,36) are evaluated for TMD DiFFs using a Gaussian approximation and for the Sivers function of Ref. [108].

Here we adopt the $\gamma^* - N$ center of mass frame, where the z axis is along the direction of the virtual photon momentum $\mathbf{q}$ and the x-z plane is defined by the lepton momenta $\mathbf{l}$ and $\mathbf{l}'$. In this frame, the transverse components of the momenta are defined with respect to the z axis with subscript $_T$ and the transverse momenta with respect to the fragmenting quark's direction with subscript $_\perp$, as demonstrated in Fig. 14 In this frame $\mathbf{p}_T = \mathbf{k}_T$, as $\mathbf{q}_T \equiv 0$ by

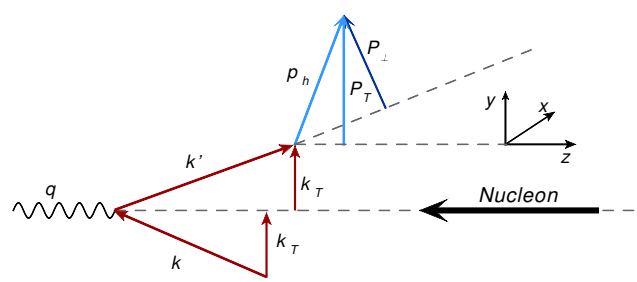

Figure 14: $\gamma^* - N$ center of mass frame.

definition. Then, similar to the single hadron production case [108], the transverse momenta of the produced hadrons to the leading twist approximation can be transformed as

$$\begin{aligned} \mathbf{P}_{1\perp} &\approx \mathbf{P}_{1T} - z_1 \mathbf{k}_T, \\ \mathbf{P}_{2\perp} &\approx \mathbf{P}_{2T} - z_2 \mathbf{k}_T. \end{aligned} \tag{38}$$

The PDF of the unpolarized quarks in the transversely polarized nucleon can be expressed as

$$f_\uparrow^q(x, \mathbf{k}_T) = f_1^q(x, k_T) + \frac{[\mathbf{S} \times \mathbf{k}_T]_3}{M} f_{1T}^{\perp q}(x, k_T), \tag{39}$$

where $f_1^q(x, k_T)$ and $f_{1T}^{\perp q}(x, k_T)$ are the unpolarized and the Sivers PDFs, respectively. Then, analogously to the single hadron case, the cross section can be factorized to PDF and DiFF terms

$$\frac{d\sigma^{h_1 h_2}}{dx \, dQ^2 \, d\varphi_S \, dz_1 \, dz_2 \, d^2\mathbf{P_{1T}} \, d^2\mathbf{P_{2T}}} = C(x, Q^2) \sum_q e_q^2 \int d^2\mathbf{k}_T \; f_\uparrow^q(x, \mathbf{k}_T) \; D_q^{h_1 h_2}(z_1, z_2, \mathbf{P}_{1\perp}, \mathbf{P}_{2\perp}), \tag{40}$$

where $C(x, Q^2) = \frac{\alpha^2}{Q^4}(1 + (1-y)^2)$ and α is the fine-structure coupling constant. We also note, that the unpolarized DiFF $D_q^{h_1 h_2}$ is here a TMD DiFFs, *i.e.* it depends on the energy

fractions and transverse components of the produced hadrons with respect to the fragmenting quark $D_q^{h_1h_2}(z_1, z_2, \mathbf{P}_{1\perp}, \mathbf{P}_{2\perp})$, as well as Q^2.

It is usually convenient to use the relative and total transverse momenta of the hadron pair as independent variables

$$\mathbf{P}_T = \mathbf{P}_{1T} + \mathbf{P}_{2T}, \tag{41}$$

$$\mathbf{R} = \tfrac{1}{2}\left(\mathbf{P}_{1T} - \mathbf{P}_{2T}\right), \tag{42}$$

where φ_T and φ_R are their corresponding azimuthal angles (note the different choice of $\mathbf{R}$ to that in the previous chapters). Then the cross section terms of the dihadron SIDIS relevant to Sviers effect can be expressed as

$$\frac{d\sigma^{h_1h_2}}{d^2\mathbf{P}_T\, d^2\mathbf{R}} = C(x, Q^2)\left[\sigma_U + S_T\left(\sigma_T \frac{P_T}{M}\sin(\varphi_T - \varphi_S) + \sigma_R \frac{R}{M}\sin(\varphi_R - \varphi_S)\right)\right], \tag{43}$$

where we suppressed the dependence of the cross-section on the rest of the variables for brevity.

Using Gaussian parametrizations for the transverse momentum dependence of PDFs and DiFFS, it has been shown explicitly in [106, 107] that both σ_T and σ_R terms are in general non-zero.

Further, in [106, 107] quantitative predictions for corresponding SSA for both $\sin(\varphi_T - \varphi_S)$ and $\sin(\varphi_R - \varphi_S)$ Sivers modulations have been made for the COMPASS experiment using an event generator. Here a widely used unpolarized event generators, `LEPTO` [109], has been modified (`mLEPTO`) to include both Cahn and Sivers azimuthal modulations of the transverse momentum of the active quark before hard scattering and hadronization [110, 111]. The resulting SSA proved to be non-wishing for both $\sin(\varphi_T - \varphi_S)$ and $\sin(\varphi_R - \varphi_S)$ Sivers modulations, and were of the same order as those for single hadron Sivers effect.

Here we employed `mLEPTO`event generator to make predictions for Sivers SSAs for dihadron SIDIS on a transversely polarized neutron target in SoLID kinematics. We employed the x, Q^2, W^2, z and missing mass $MM_{e'\pi^+\pi^-}$ described in Section 3.3. We also put cuts on polar angles of the produced pions in the lab system 8 to 15 degrees, and on the scattered electron 8 to 15 and 16 to 24 degrees. Here we present the results only for 11 GeV electron beam. While we show the results for a neutron target, they can be repeated for a proton target, as should be tested elsewhere.

On Fig. 15 the histograms describe the distribution of the flavour of the struck quark for the events selected after the cuts. The histograms are normalized with the number of mLEPTO generated events. We see that the relative contribution of the d quark for producing $\pi^+\pi^-$ pairs increases in neutron with respect to proton. Thus measurements of the Sivers SSAs of this proposal would help to pin down the Sivers PDF of the d quark.

The plots in Fig. 16 depict the x-dependences of the Sivers SSAs for $\pi^+\pi^-$ pairs produced on neutron and proton targets respectively. Here we impose on each hadron a $z_i > 0.1$ cut, along with the cuts on the total $0.3 < z < 0.9$ coming from the kinematics. "T" and "R" denote SSA corresponding to the Sivers type modulation of the total and relative transverse momenta of the hadron pair. We see that these SSAs for neutron have opposite sign, due to the significant contribution of the d quark.

The plots in Fig 17 depict the z-dependences of the Sivers SSAs. The plots with legend "Cut" denote additional cuts on the momentum of π^+, i.e. $z_1 > 0.3$, $P_{1T} > 0.3GeV$. This cut reduces the statistics, but enhances the SSAs.

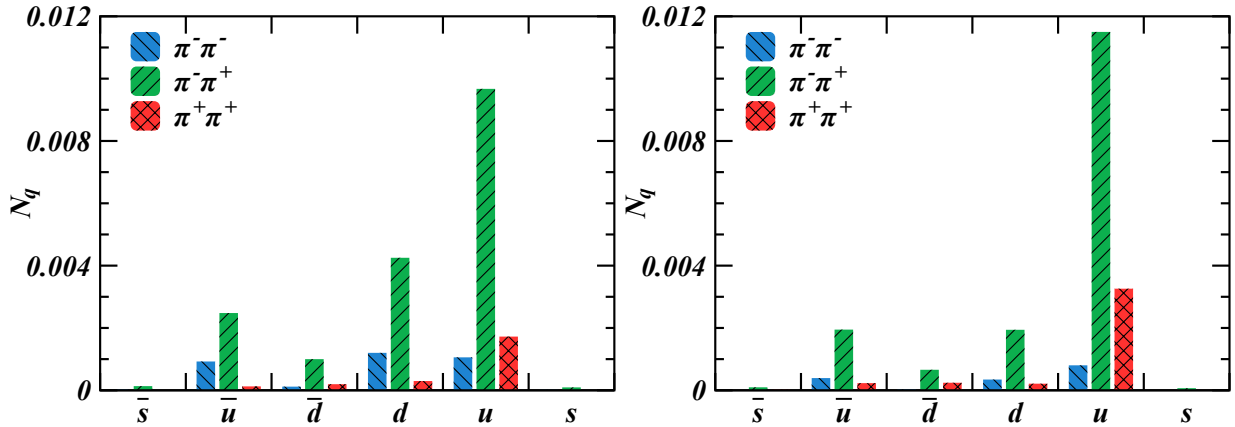

Figure 15: Relative rates for the struck quark flavor in events that produce a given type hadron satisfying the SoLID kinematics. For a neutron target (left panel) and proton target (right panel).

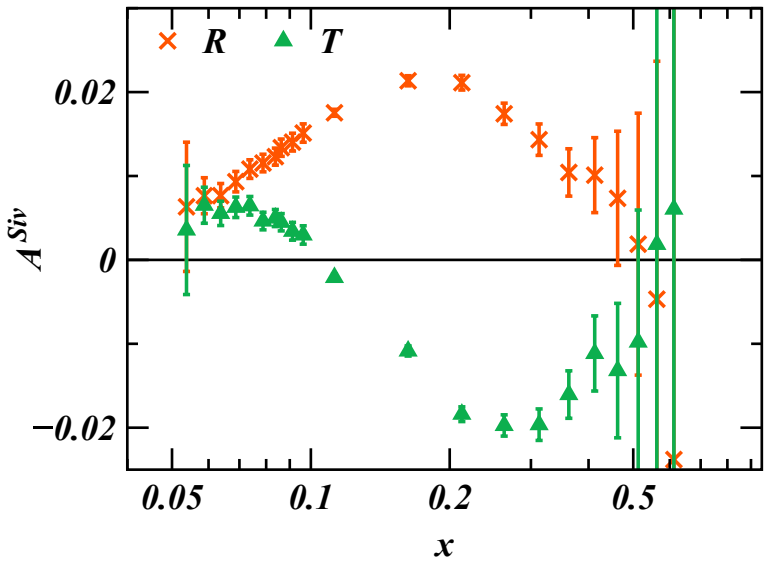

Figure 16: The x dependence of the Sivers asymmetry for the SoLID kinematics. Here for a neutron target.

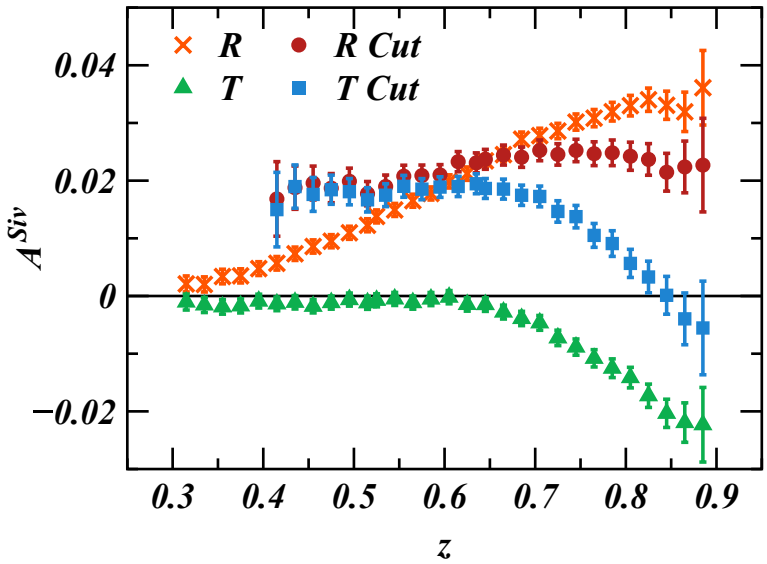

Figure 17: The z dependence of the Sivers asymmetry for the SoLID kinematics. Here for a neutron target.

These predictions demonstrate the viability of such complementary extraction of Sivers-type SSAs from the same data set to be used in the extraction of the SSAs involving the transversity PDF. This measurement will provide significant new information for extraction of Sivers PDF in global combined fits.

3 The proposed experiment

3.1 Overview

We proposed to measure the electroproduction hadron pairs using the Solenoidal Large Intensity Device (SoLID). SoLID have two configurations of setup corresponding to two group of experiments which are using it. One configuration is named SoLID-PVDIS which is for the parity violation in deep inelastic scattering (PVDIS) experiment E12-10-007 [112]. The other configuration is named SoLID-SIDIS, which is for semi-inclusive deep inelastic scattering (SIDIS) experiments: E12-10-006 [113], E12-11-007 [114] and E12-11-108 [115]. There is one more experiment E12-12-006 [116], which will also use SolID-SIDIS configuration with very small modification. All these experiments have been approved with A or A^- rating. This new experiment will use identical setup as E12-10-006 and run parallel to it. E12-10-006 aims to measure the scattered electron with one pion electroproduction coincident events from the transversely polarized ^{3}He target, while this experiment is focus on measuring the triple coincident events of the scattered electron with one negative pion and one positive pion from the same target.

The layout of the SoLID is shown in Fig. 18. The detector system consists of two parts: the forward angle detector system and the large angle detector system. The forward angle detector system has a polar angle coverage from 8° to 15°, it can identify charge particles with momenta above 0.8 GeV/c. Particle's tracking in the forward angle region is provided by 5 layers of Gaseous Electron Multipliers (GEMs). Particles can be identified from a combination of the forward angle electromagnetic calorimeter (FAEC), a gas Cerenkov counter (CC), and a layer of Multi-gap Resistive Plate Chamber (MRPC). The large angle detector system covers the polar angle from 16° to 24°. The large angle electromagnetic calorimeter (LAEC) is a radiation resistant "shashlyk"-type calorimeter and can be used in the magnetic field. In order to suppress the photon background, a scintillator layer will be built in front of the LAEC. Combining the signal from GEMs and LAEC will suppress the photon background even better.

The reaction of interest is $\mathrm{n}^\uparrow(e, e'\pi^+\pi^-)\mathrm{X}$, where e' is the scattered electron which will be detected through either the forward angle detector system or the large angle detector system, and the two pions are detected only by the forward angle detector system. We plan to use a 15 μA beam with 11 GeV and 8.8 GeV energies.

The main goal of this experiment is to measure the x, Q^2, $M_{\pi^+\pi^-}$ and $z_{\pi^+\pi^-}$ dependencies of the target single-spin asymmetries. The target single spin asymmetry, A_{UT}, will be calculated in bins of $\sin(\phi_R + \phi_S)$ and $\sin\theta$ as Eq.(44):

$$A_{UT}(\phi_R, \theta) \;=\; \frac{1}{fP_t}\frac{(N^+ \;-\; N^-)}{(N^+ \;+\; N^-)}\;, \tag{44}$$

where P_t is the target polarization (with respect to the electron beam direction), f is the dilution factor, i.e. the fraction of events from the polarized material of interest (neutron), and $N^{+(-)}$ are the charge-normalized extracted number of $en^\uparrow \to e\pi^+\pi^-X$ events for opposite orientations of the transverse spin of the target.

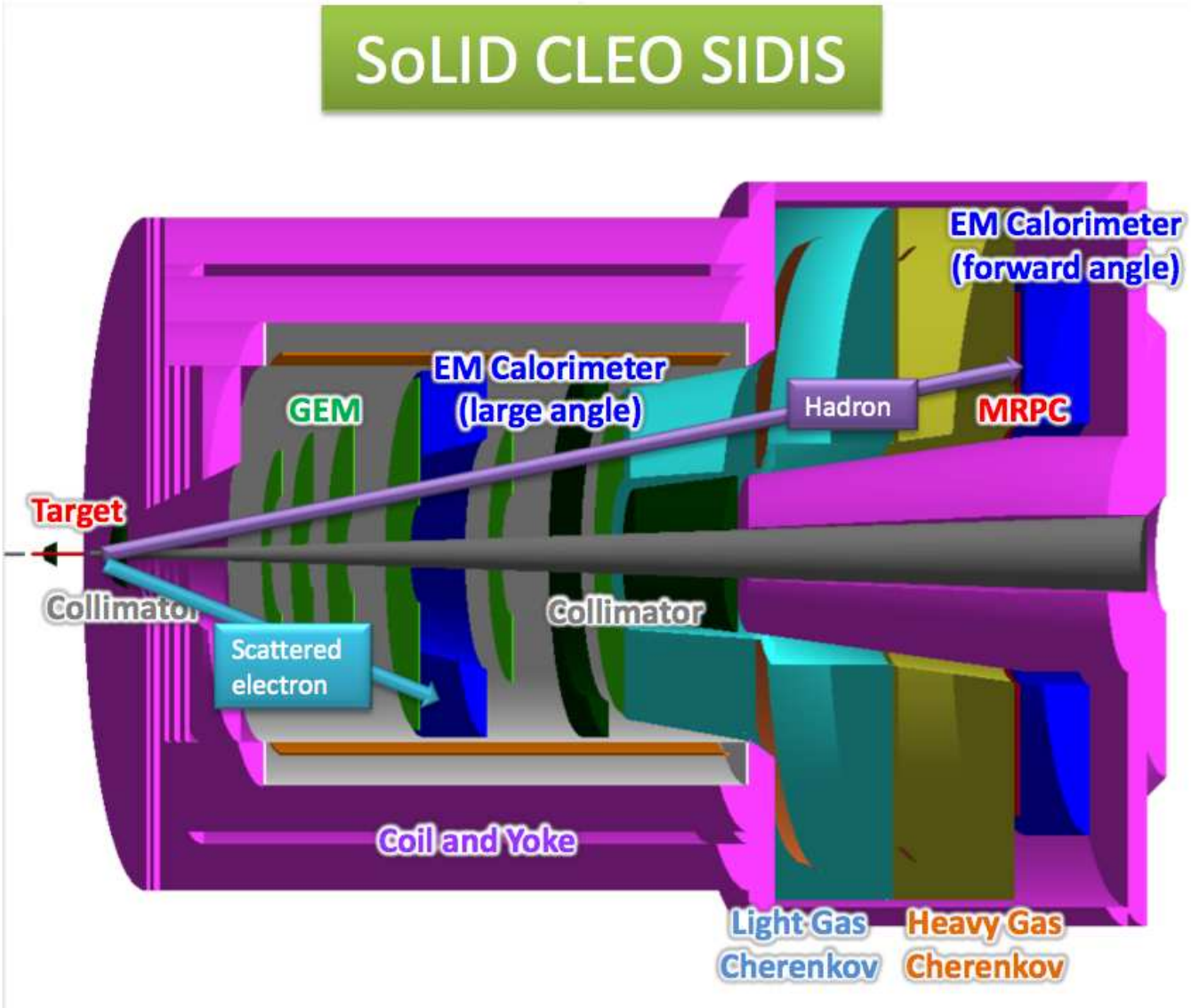

Figure 18: The experimental layout of SoLID in SIDIS configuration with CLEO magnet. The sub-detectors are labeled and the final state particles are illustrated by arrows. The scattered electron are detected by both the forward angle detectors and the large angle detectors. The hadrons can be detected by the forward angle detectors. There are five layers of Gaseous Electron Multipliers (GEMs) inside the CLEO coils located upstream of the gas Cherenkov Counter (CC). The forward angle electromagnetic calorimeter (FAEC) provides the trigger and an additional electron/pion separation. The Multi-gap Resistance Plate Chamber (MRPC) provides time of flight information. The large angle electromagnetic calorimeter (LAEC) provides the trigger, the coincidence timing and the electron/pion separation. The 40 cm long ^{3}He target is located at z = -350 cm relative to the center of the CLEO coil. The target collimator will shield high energy photon and electrons from the end cap of the target vessel.

3.2 The polarized ^{3}He target

The polarized ^{3}He target system is based on the technique of spin-exchange between optical pumped hybrid Rubidium-Potassium atoms and ^{3}He atoms. This target has been used successfully in a number of Hall A 6 GeV experiments. It recently achieved an in-beam averaged polarization of 55-60% in the experiment of E06-010 [117]. The target cell is 40 cm long and is filled with 10 amg (10 atm at 0° C) ^{3}He gas. 15 μA of beam current is allowed on the target in order to have a relative small target depolarization and also keep a long life time for the target cell. The luminosity is about 10^{36} nuclei/s/cm^2. The target polarization are measured by both NMR and Electron Paramagnetic Resonance (EPR). The uncertainty of these 2 polarimetries are about 3% [113]. In this experiment, the target will be located 350 cm upstream from the coil center.

3.3 Kinematics

We are running a Geant4 based simulation program for SoLID. The total momentum and polar angle coverages of the scattered electron and pions are shown in Fig 19. We applied energy threshold cut of 3.0 GeV in LACE and 0.8 GeV in FAEC, which remove a lot of low energy electron-like triggers in LAEC. The electron polar angle coverage is from 8° to 15° in the forward detector system and 16° to 24° . The polar angle coverage for hadrons is also 8° to 15° .

In this experiment, we are interested in the dihadron production only in the DIS region. To ensure the DIS kinematics, we will apply cuts for $Q^2 > 1$ (GeV/c)^2, $W > 2.3$ GeV and $MM_{e'\pi^+\pi^-} > 1.414$ GeV (missing mass of the dihadron reaction) to avoid the resonance region. In order to choose dihadron reaction from the current fragmentation instead of from the target fragmentation, we require $0.3 < z_{\pi^+\pi^-} < 0.9$, where $z_{\pi^+\pi^-}$ is the energy fraction of these two pions to the total energy transfer. This will ensure that these two pions are the leading hadrons in the event. We also require $MM_{e'\pi^+\pi^-} > 1.414$ GeV/c, where $MM_{e'\pi^+\pi^-}$ is the missing mass of the reaction of $\mathrm{n}^{\uparrow}(e, e'\pi^+\pi^-)\mathrm{X}$, to remove the exclusive events. Please note that our kinematic cuts are different from those used in E12-10-006 in terms of z and missing mass. They require $0.3 < z_\pi < 0.7$ and $MM_{e\pi} > 1.6$, while Q^2 and W are cut at the same range as us. The final kinematic coverages in this experiment will be $x = 0.05$ - 0.65, $Q^2 = 1.0$ - 8.0 (GeV/c)^2, $M_{\pi^+\pi^-} = 0.28$ - 1.5 GeV/c and $z_{\pi^+\pi^-} = 0.3$ - 0.9. Their ranges are shown in Fig 20 for 11 Gev electron beam energy and Fig 21 for 8.8 GeV electron beam. We choose to map the data into 9 bins in x, 5 bins in Q^2, 7 bins in $M_{\pi^+\pi^-}$ and 6 bins in $z_{\pi^+\pi^-}$. These bin boundaries are also shown in the figures. In total we have about 700 bins that have observable statistics. The weighted central values of these bins are also listed in Table. 1.

3.4 Rates

The expected single electron rate and electron plus one single pion coincident rates have been estimated for E12-10-006 and show in Table.3 in [113]. But the design of SoLID has been changed since then. The CLEO-II magnet was finally chosen to to be the magnet for SoLID. The polar angle coverage is now from 8° - 15° for the forward detector system,

comparing 6.6° - 12° in the past. The polar angle coverage for the large angle detector system is now 16° - 24° other than 14.5° - 22° . For details of the current design of SoLID, please refer to [118]. Due to these changes we will expect lower event rates in the single electron and background. Therefore we only re-estimate the rates for the single pion coincident events and the dihadron coincident events of this experiment.

A Geant4 based simulation program, GEMC-SoLID, is used in this study. The target collimator effect has been taken into account in the GEANT4 simulation for the acceptance. We are still assuming 15 μA beam current, a 40 cm long gaseous ^{3}He at 10 amagats, which will provide a beam and target luminosity of 10^{36} (n)/cm^2/s. The averaged target polarization is assumed to be 60%. An effective neutron polarization of 86% in ^{3}He ground state is also considered. The overall detector efficiency is assumed to be 85%, including the detector efficiency and DAQ dead time.

This experiment will use the same trigger as E12-10-006, which is the coincident of one electron from either forward angle or large angle detectors system and one hadron from the forward angle detector system. The electron and pion coincident rates are estimated with PEPSI event generator [119]. The updated single pion coincidence rates and double pion coincident rate can be found in Table. 3.4. The applied low momentum cuts are 0.8 GeV/c for the forward angle detectors and 3.0 GeV/c for the large angle detectors, which are basically corresponding to the trigger threshold.

Process	Rates at 11 GeV	Rate at 8.8 GeV
n$(e, e'\pi^{\pm})$	1.87 kHz	1.21 kHz
n$(e, e'\pi^{+})$	1.05 kHz	0.61 kHz
n$(e, e'\pi^{-})$	0.87 kHz	0.56 kHz
n$(e, e'\pi^{+}\pi^{-})$	0.26 kHz	0.08 kHz

Table 2: The estimated coincidence rates (under kinematics cuts) from polarized neutron with 11 and 8.8 GeV electron beam.

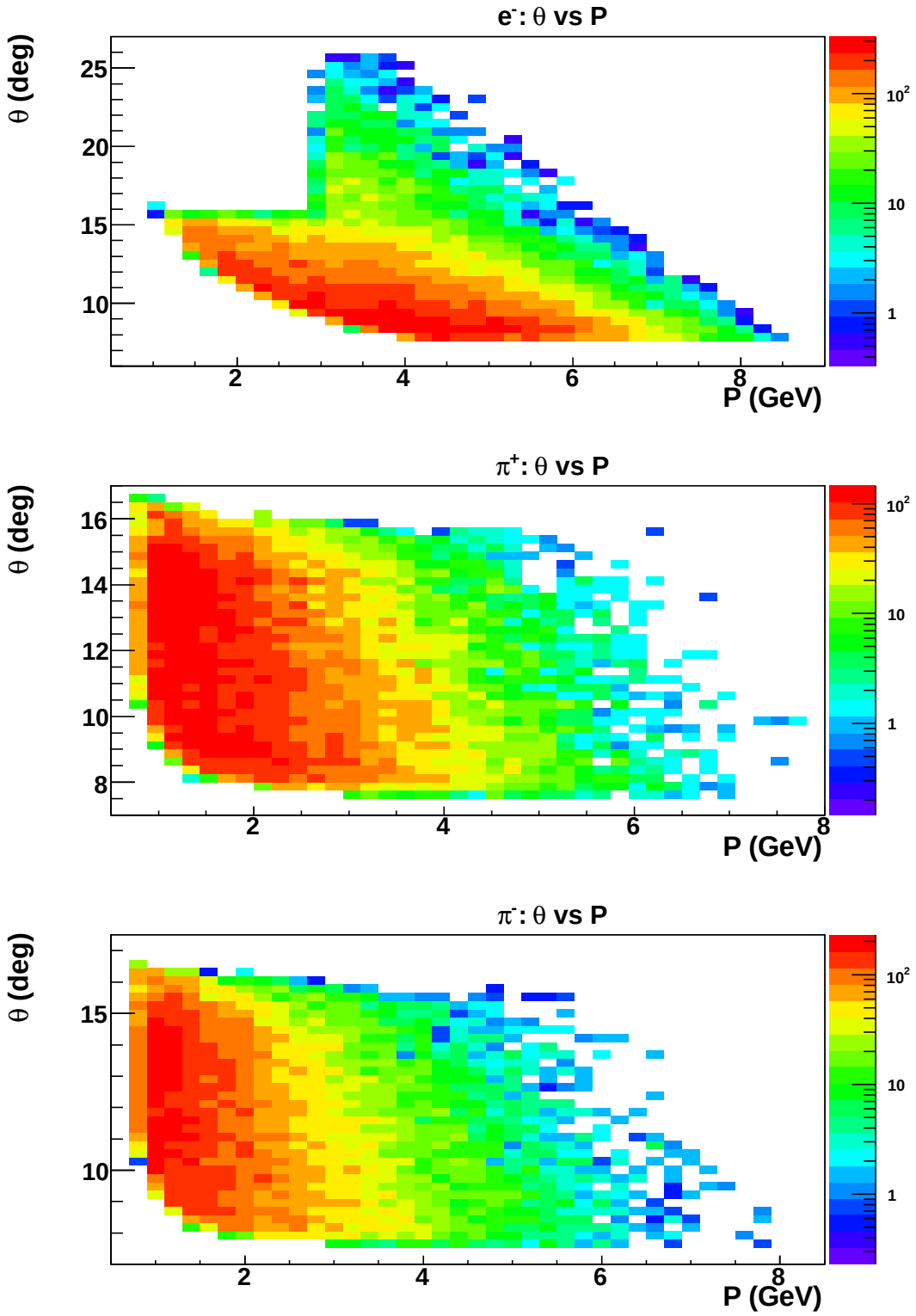

Figure 19: Polar angle and momentum coverages in this experiment for scattered electrons, positive pions and negative pions. Trigger energy threshold cut of 0.8 GeV and 3.0 GeV have been applied to the forward angle and large angle detector system, respectively.

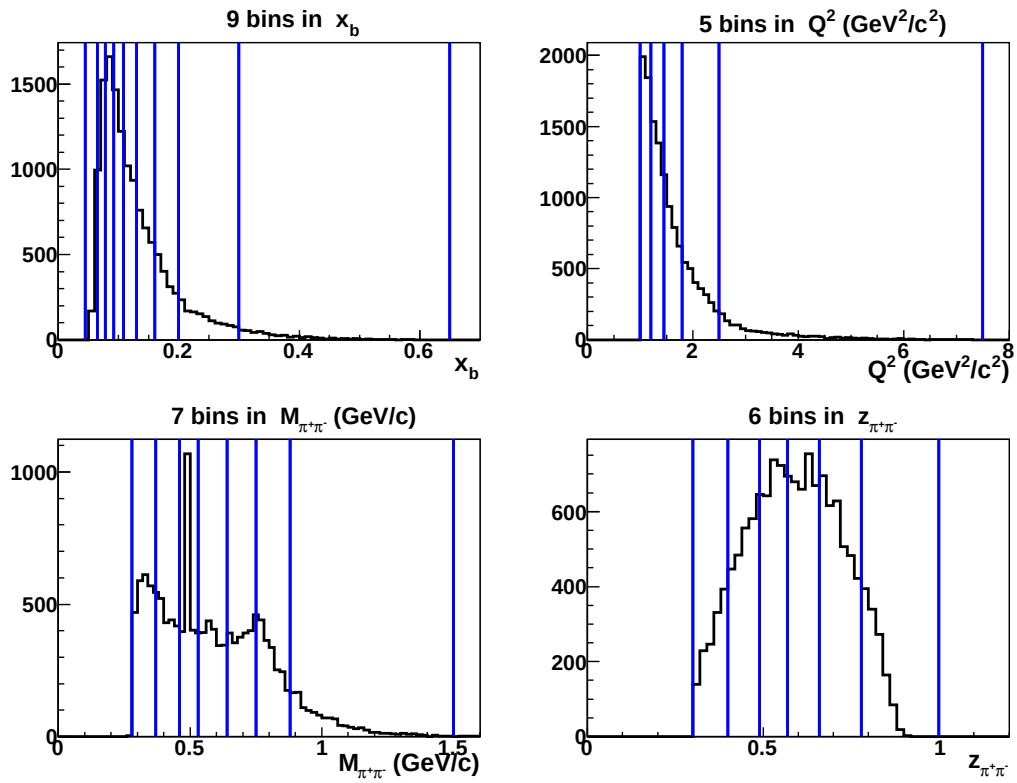

Figure 20: Kinematics coverages for the $n^{\uparrow}(e, e'\pi^+\pi^-)X$ with 11 GeV electron beam energy. The boundaries of each bin are indicated with blue vertical lines.

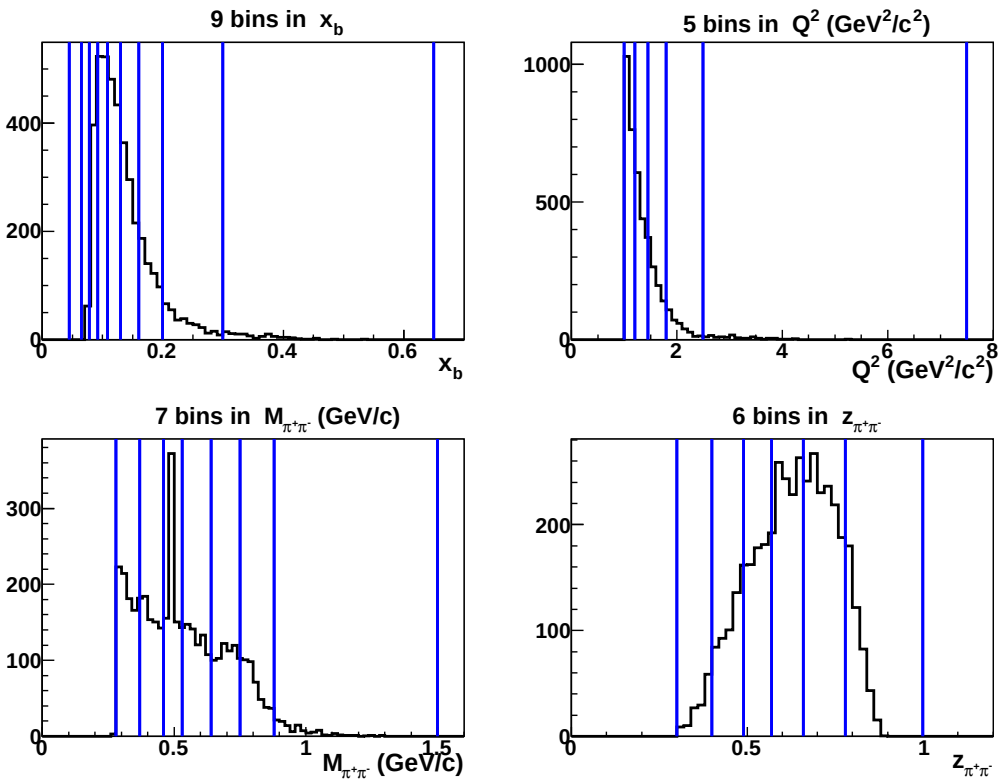

Figure 21: Kinematics coverages for the $n^{\uparrow}(e, e'\pi^+\pi^-)X$ with 8.8 GeV electron beam energy. The boundaries of each bin are indicated with blue vertical lines. We choose the same bin width for both 11 GeV data set and 8.8 GeV data set.

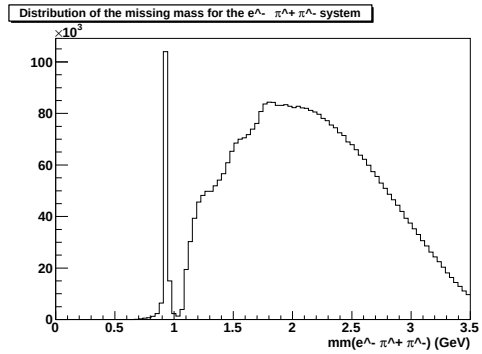

Figure 22: Missing mass distribution for pion pairs dihadron events from PEPSI. Feimi motion effects is not considered yet.

Table 3: Uncertainties for asymmetry measurements.

sources	δA_{UT}
background subtraction	5%
target polarization	3%
dilution factor	1%
nuclear effect	4%
radiative corrections	2%
total systematic uncertainty	7.4%

4 Systematic errors

Systematic uncertainties due to SoLID acceptance effects have been studied using the PEPSI generator and the Geant4 simulation program, GEMC-SoLID. QED radiative effects were not turned on in PEPSI since it is known to be small. A target polarization of 60% is assumed.

The kinematic cuts considered for these projections are the following: $Q^2 > 1.0$ (GeV)^2, $W > 2.3$ GeV, $MM_{e'\pi^+\pi^-} > 1.414$ GeV, and $0.3 < z_{\pi^+\pi^-} < 0.9$.

The missing mass distributions for different hadron pair combinations are shown in Fig. 22. A cut on the missing mass of the dihadron pairs, $MM_{e'\pi^+\pi^-} > 1.414$ GeV/c, is applied in order to suppress contamination from exclusive production.

The systematic uncertainties due to cuts described above are identified as background subtraction. We estimated it to be in a 5% level. Other sources of systematic errors include a 3% the target polarizations uncertainty, and a 1% target dilution factor uncertainty, 4% nuclear effects from ^{3}He and about 2% due to radiation correction. The main sources of systematic errors in this SSA measurement are listed in Table 3. To estimate the total systematic error, we have added the systematic errors from the various contributions in quadrature. The total uncertainty is expected to be in a level of 7.4%.

5 Projected results

The projected statistical errors for polarized neutron target asymmetries are based on the assumption of running 48 days with 11 GeV and 24 days with 8.8 GeV.

Fig. 23- 29 show the statistics error in all 3-Dimensional (3-D) bins of accessible phase space (x, Q^2, $z_{\pi^+\pi^-}$), varying in $M_{\pi^+\pi^-}$ from 0.34 to 1.15, for transverse target spin asymmetry A_{UT} from a neutron target, corresponding to 48 days of data-taking with 11 GeV beam and 24 days of 8.8 GeV beam.

We also present the 1-D statistical precision of the A_{UT} asymmetries for pion pairs as a function of x, $M_{\pi^+\pi^-}$, and $z_{\pi^+\pi^-}$ in Fig. 30 for 11 GeV beam energy. These 1-D A_{UT} are integrated over the other 3 variables bins. The error bands represent the upper and lower limits of different model calculations shown in Fig. 10.

Fig. 31 shows the $h_1^u(x)$ and $h_1^d(x)$ distribution, separately, as a function of x from COMPASS data, combining the proton 2007 and deuteron 2002-2004 data. The result from this experiment combining with the proton dihadron measurement from CLAS12 (PR12-12-009) and SoLID(E12-11-108) will provide much precise data and also extend to higher x (about 0.6), where is dominated by valence quarks.

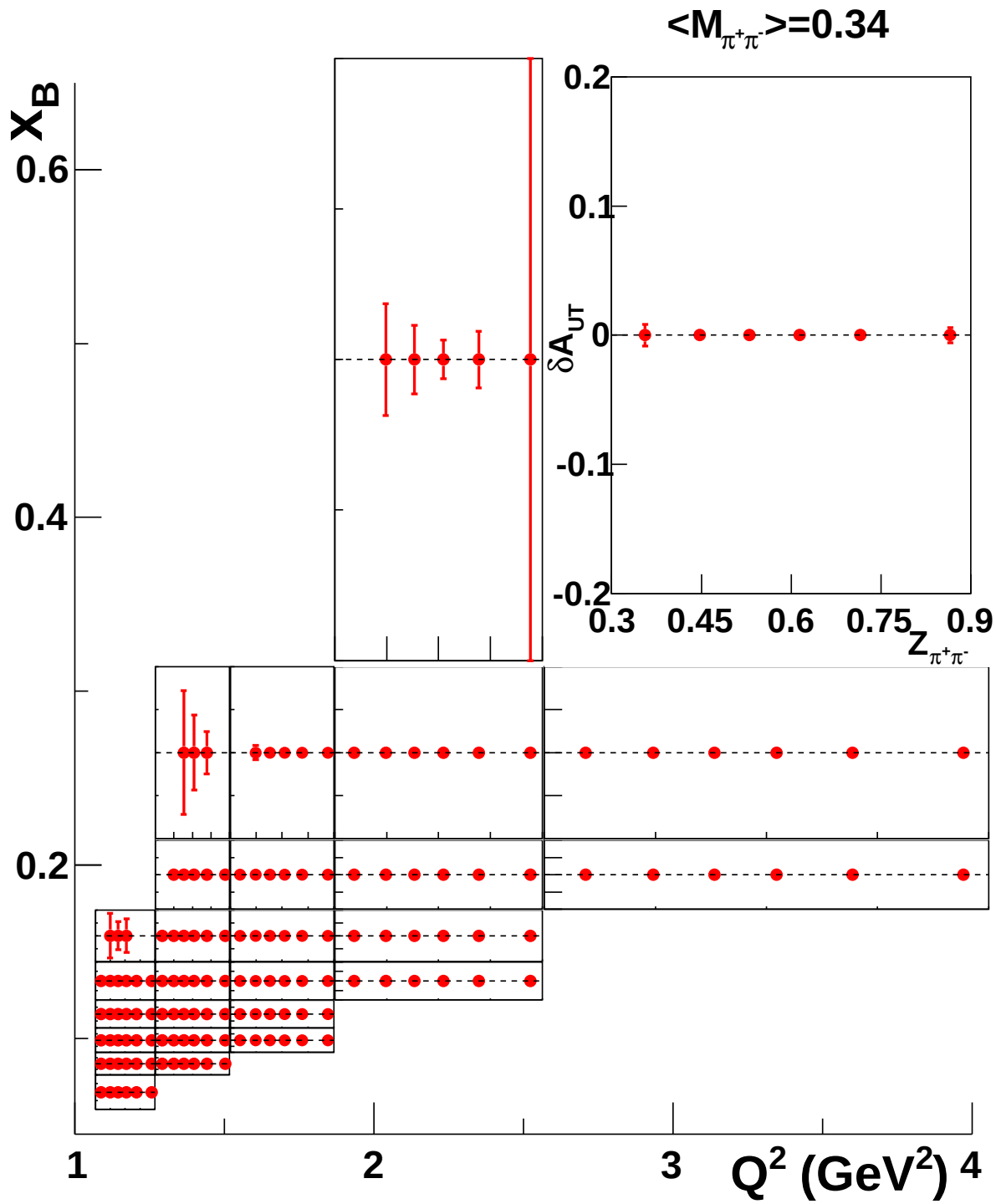

Figure 23: The projected statistics errors for each 3-D bin(x, Q^2, $z_{\pi^+\pi^-}$) with $M_{\pi^+\pi^-}$ =0.34. The external square is corresponding to x (vertical) and Q^2 (horizontal). The internal squares are corresponding to the statistics error of A_{UT} at that 3-D bin vs $z_{\pi^+\pi^-}$, whose ranges are illustrated in the top right panel. All internal panels have the same ranges in both horizontal and vertical axis.

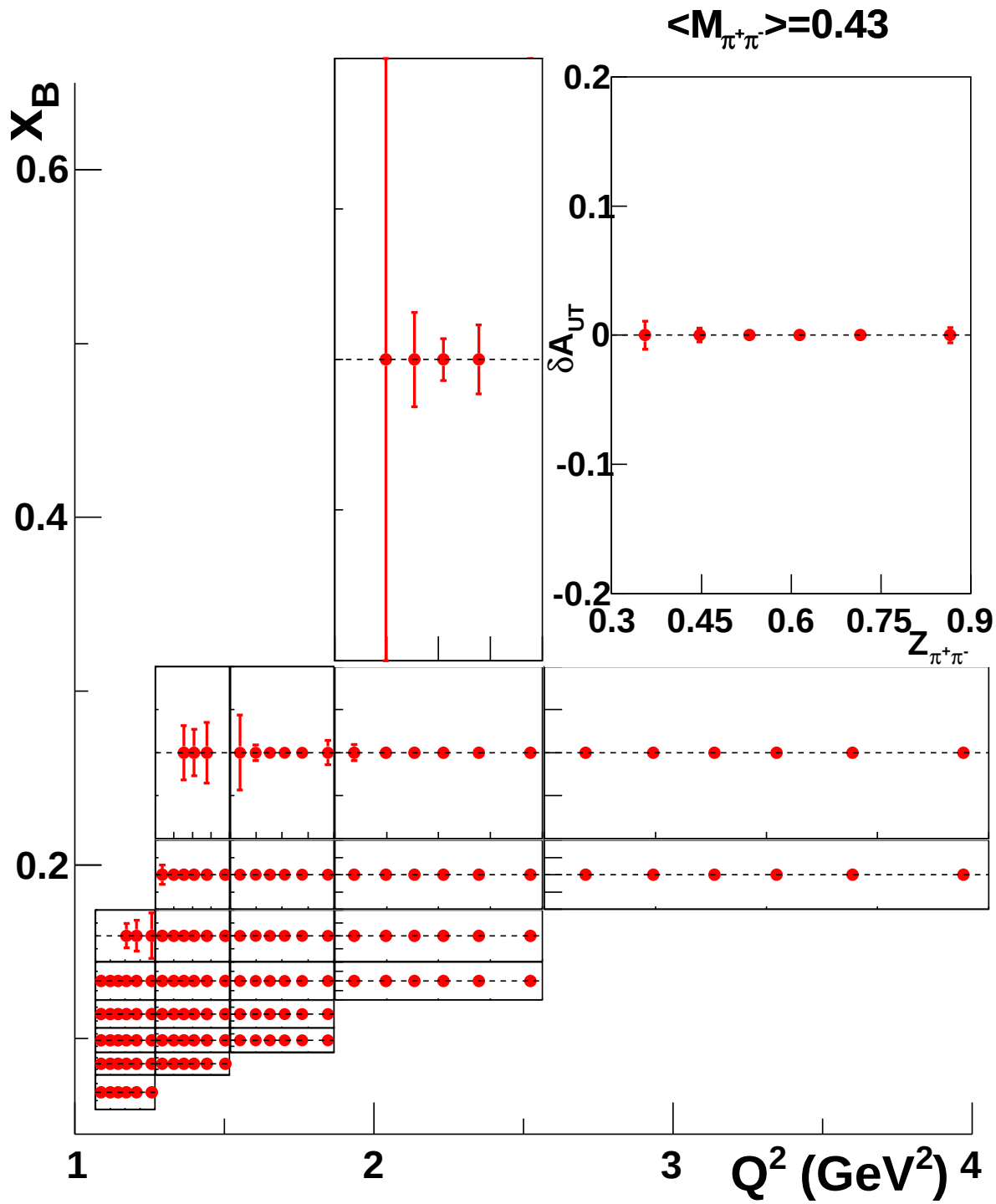

Figure 24: The projected statistics errors for each 3-D bin(x, Q^2, $z_{\pi^+\pi^-}$) with $M_{\pi^+\pi^-}$ =0.43. The external square is corresponding to x (vertical) and Q^2 (horizontal). The internal squares are corresponding to the statistics error of A_{UT} at that 3-D bin vs $z_{\pi^+\pi^-}$, whose ranges are illustrated in the top right panel. All internal panels have the same ranges in both horizontal and vertical axis.

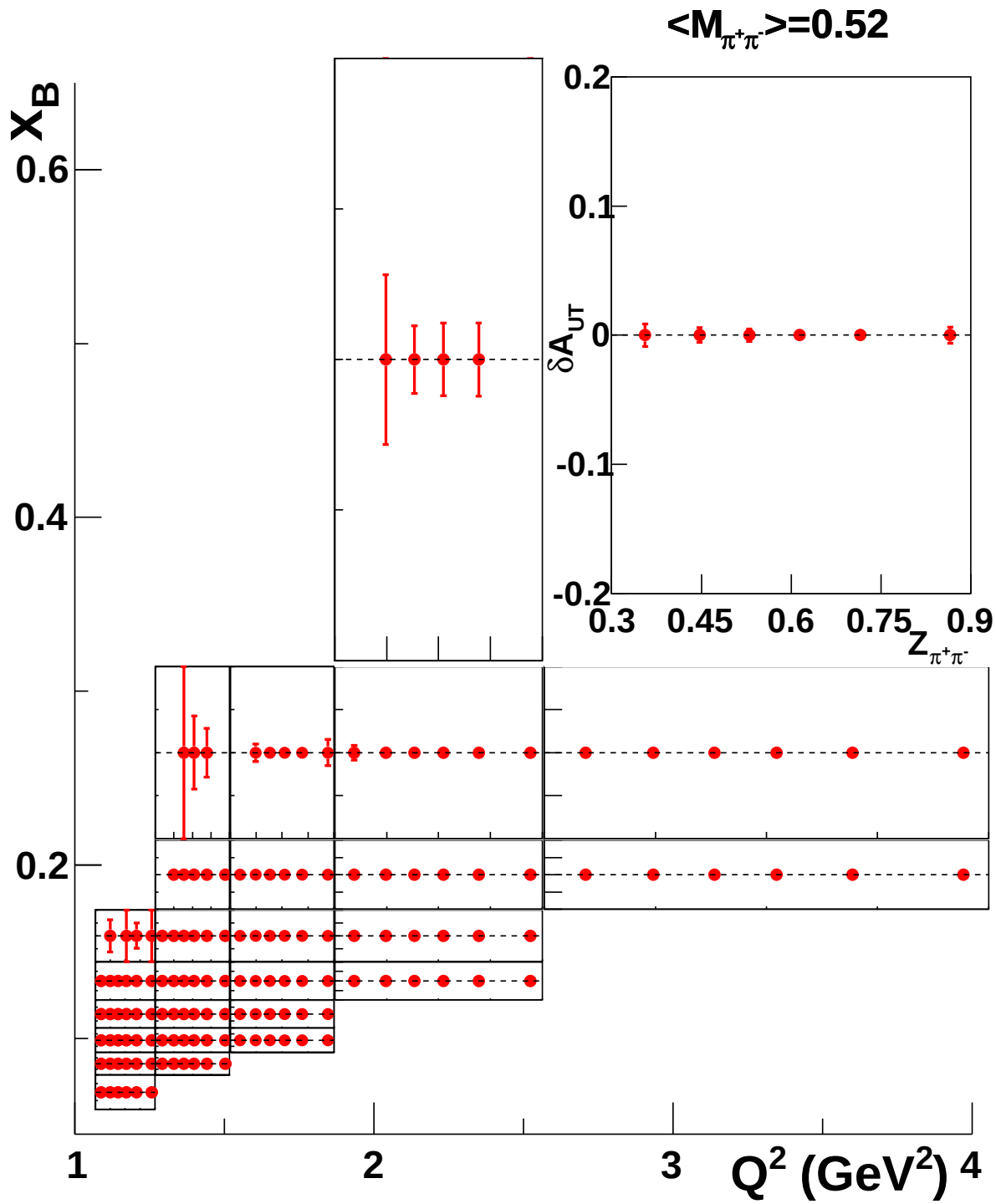

Figure 25: The projected statistics errors for each 3-D bin(x, Q^2, $z_{\pi^+\pi^-}$) with $M_{\pi^+\pi^-}$ =0.52. The external square is corresponding to x (vertical) and Q^2 (horizontal). The internal squares are corresponding to the statistics error of A_{UT} at that 3-D bin vs $z_{\pi^+\pi^-}$, whose ranges are illustrated in the top right panel. All internal panels have the same ranges in both horizontal and vertical axis.

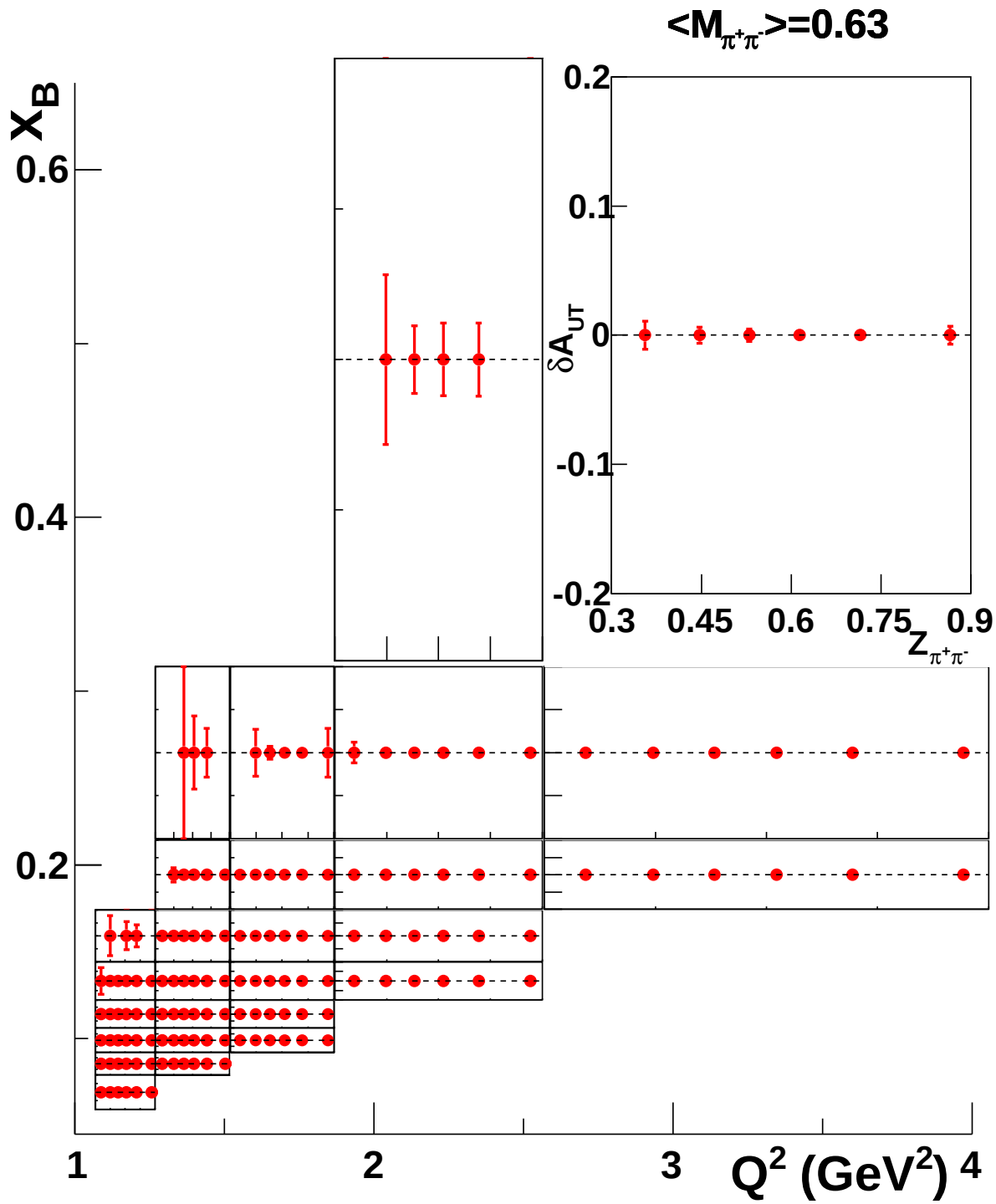

Figure 26: The projected statistics errors for each 3-D bin(x, Q^2, $z_{\pi^+\pi^-}$) with $M_{\pi^+\pi^-}$ =0.63. The external square is corresponding to x (vertical) and Q^2 (horizontal). The internal squares are corresponding to the statistics error of A_{UT} at that 3-D bin vs $z_{\pi^+\pi^-}$, whose ranges are illustrated in the top right panel. All internal panels have the same ranges in both horizontal and vertical axis.

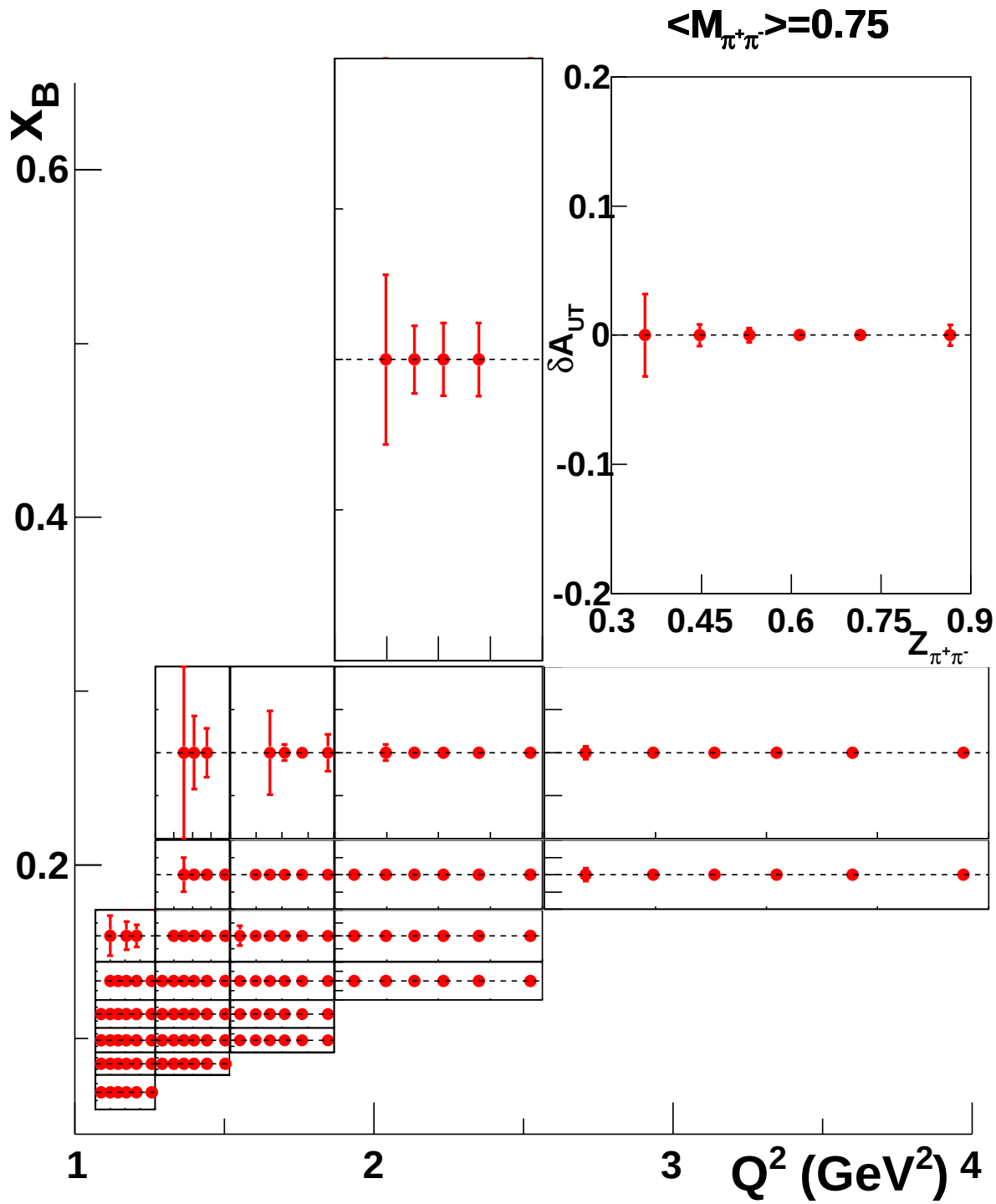

Figure 27: The projected statistics errors for each 3-D bin(x, Q^2, $z_{\pi^+\pi^-}$) with $M_{\pi^+\pi^-}$ =0.75. The external square is corresponding to x (vertical) and Q^2 (horizontal). The internal squares are corresponding to the statistics error of A_{UT} at that 3-D bin vs $z_{\pi^+\pi^-}$, whose ranges are illustrated in the top right panel. All internal panels have the same ranges in both horizontal and vertical axis.

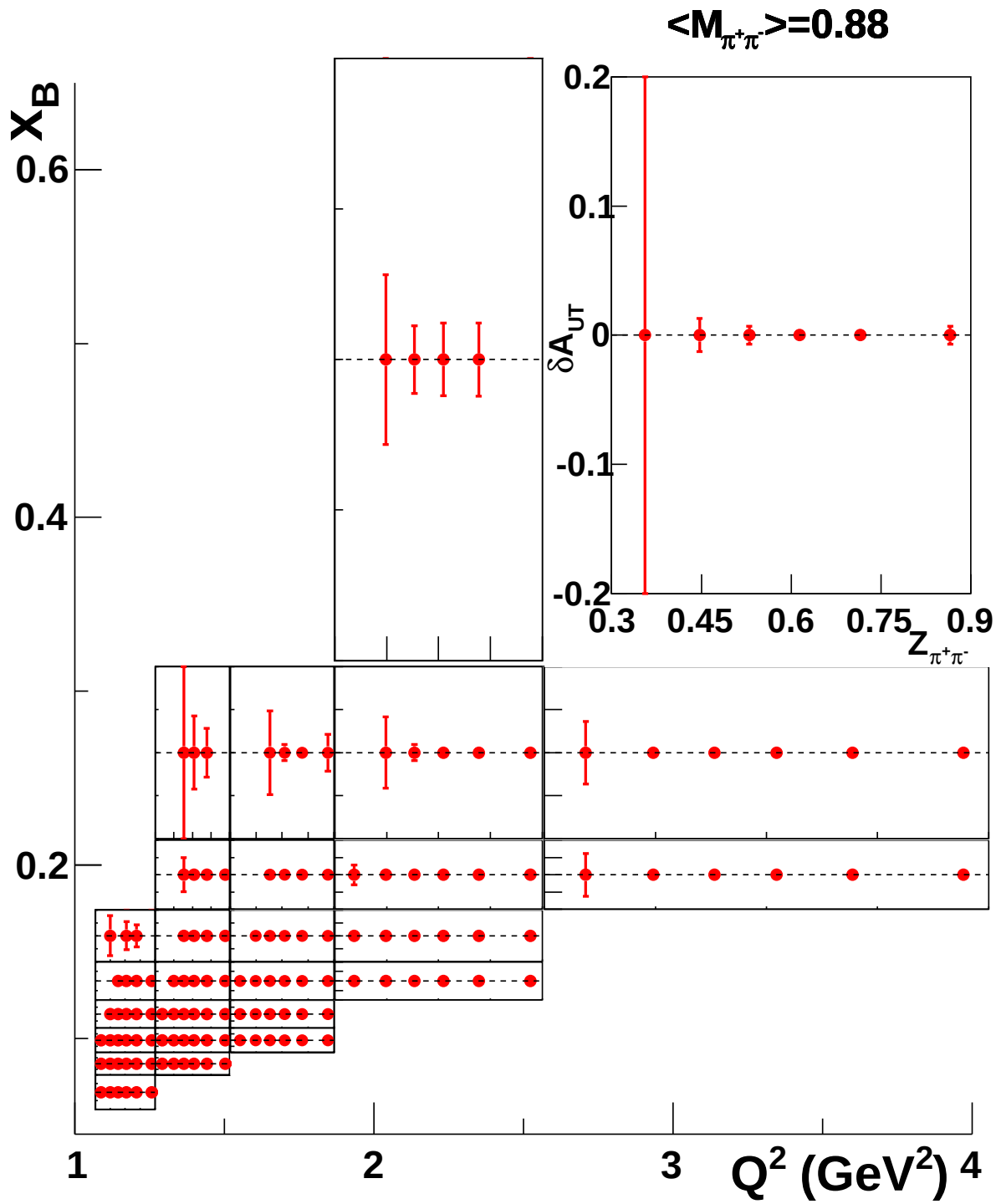

Figure 28: The projected statistics errors for each 3-D bin(x, Q^2, $z_{\pi^+\pi^-}$) with $M_{\pi^+\pi^-}$ =0.88. The external square is corresponding to x (vertical) and Q^2 (horizontal). The internal squares are corresponding to the statistics error of A_{UT} at that 3-D bin vs $z_{\pi^+\pi^-}$, whose ranges are illustrated in the top right panel. All internal panels have the same ranges in both horizontal and vertical axis.

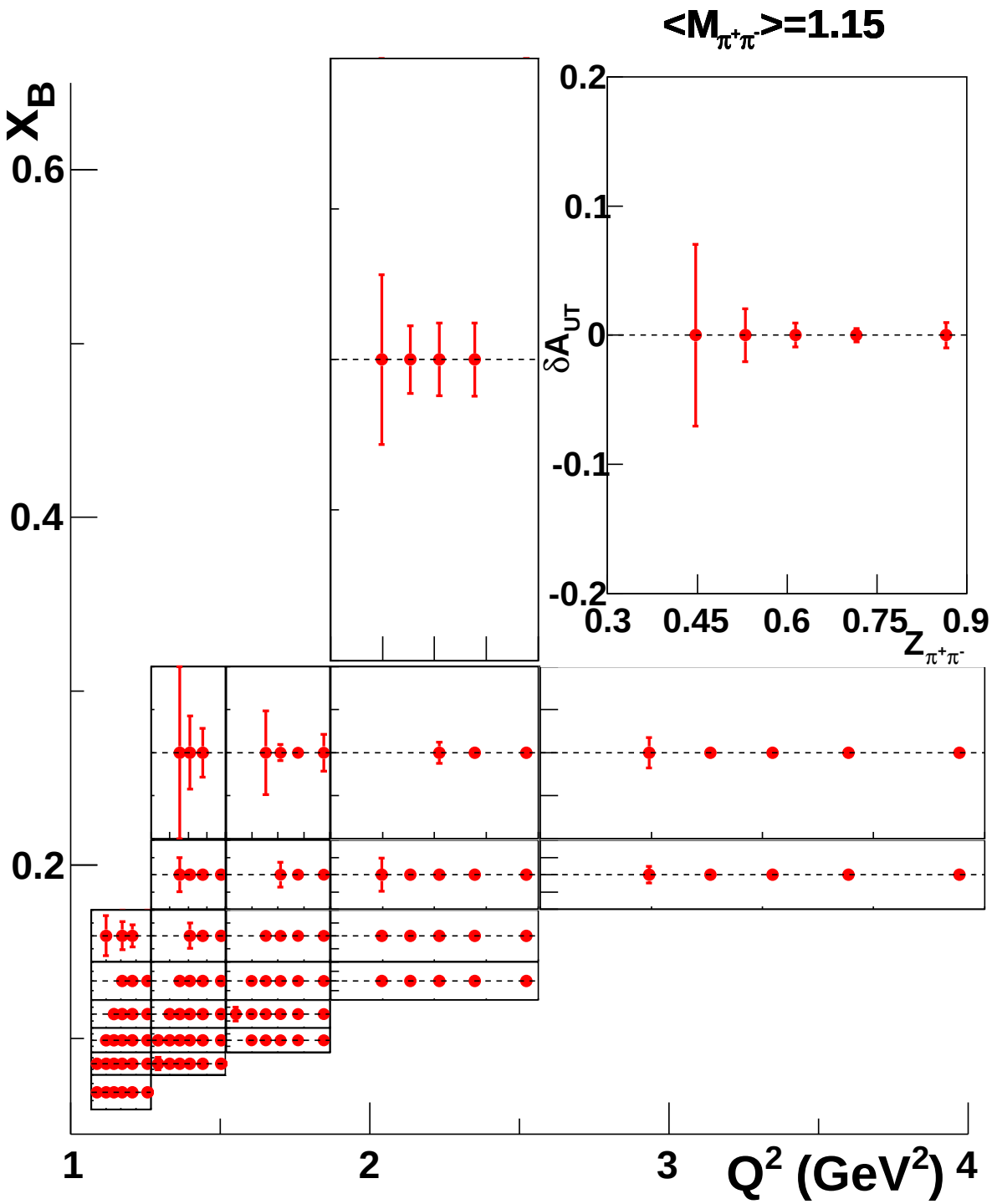

Figure 29: The projected statistics errors for each 3-D bin(x, Q^2, $z_{\pi^+\pi^-}$) with $M_{\pi^+\pi^-}$ =1.15. The external square is corresponding to x (vertical) and Q^2 (horizontal). The internal squares are corresponding to the statistics error of A_{UT} at that 3-D bin vs $z_{\pi^+\pi^-}$, whose ranges are illustrated in the top right panel. All internal panels have the same ranges in both horizontal and vertical axis.

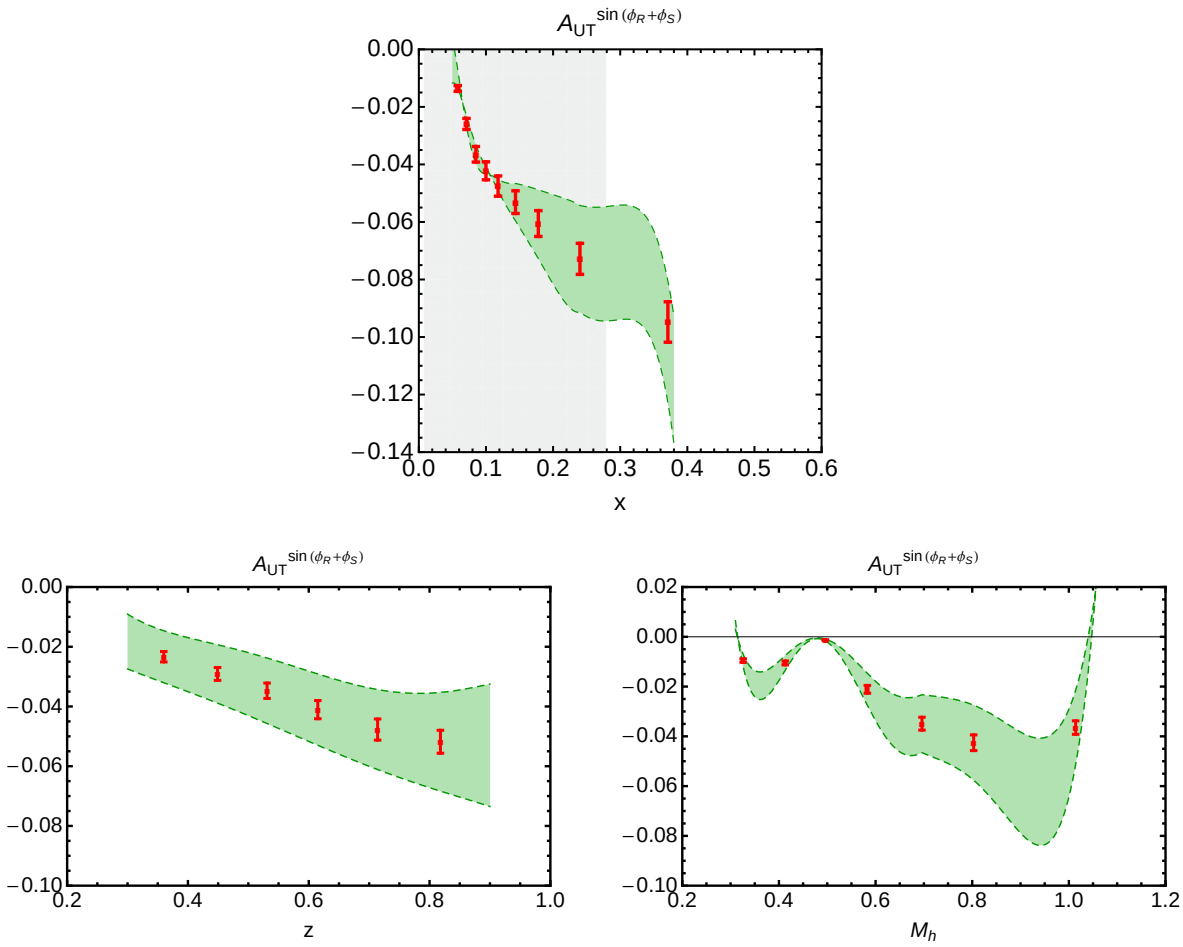

Figure 30: The projected statistical and systematical errors for data on a neutron target (48 days with 11 GeV at SoLID) for the target asymmetry $A_{UT}^{\sin(\phi_R+\phi_S)}$ in (x, $z_{\pi^+\pi^-}$, $M_{\pi^+\pi^-}$). The band represent the spread in predictions using the TMD extraction (2009) and the collinear extraction for $h_1(x)$. The DiFFs and PDFs are evolved to the corresponding value of Q_2 for each bin except for the TMD extraction for $h_1(x, k_\perp)$. The DiFFs variables (z, M_h) are integrated over the range corresponding to each bin. The grey area on the x 1D projection correspond to the range of available data from HERMES and COMPASS. Both the TMD and the collinear fits are valid within that range only.

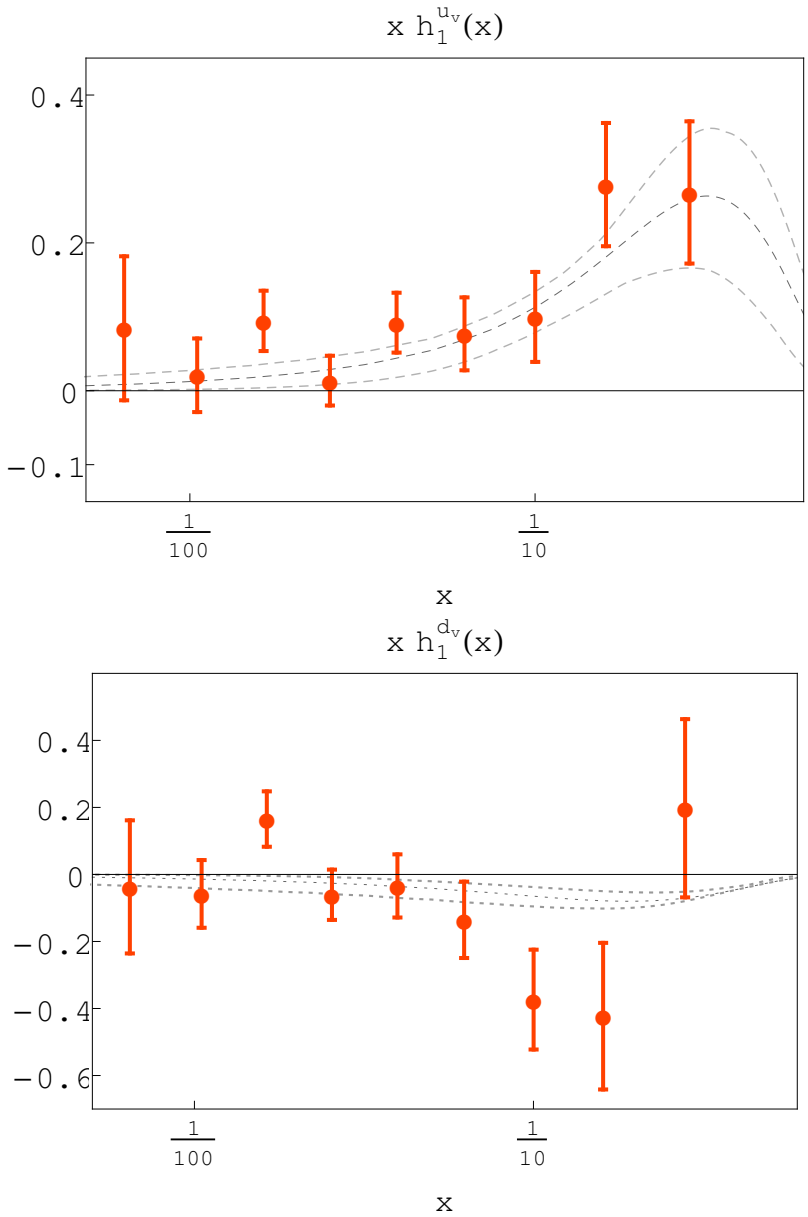

Figure 31: The transversity distribution, $h_1^u(x)$ (top) and $h_1^d(x)$ (bottom) as a function of x, extracted from COMPASS proton 2007 and deuteron 2002-2004 data via DiFFs [93, 34]. The grey curves correspond to the Torino extraction with error bands. This proposal will provide much precise data and also extend x up to 0.6.

6 Beam time request

The beam time requested is listed in Table 4. A total of 90 days of beam time with 15 μA, 11/8.8 GeV electron beams have been requested by E12-10-006. 72 days is for beam on the polarized ^{3}He target. In addition, 10 days are requested for dedicated study of the naive $x-z$ factorization with hydrogen and deuterium gas using our reference cell. A total overhead time of 8 days are requested, which includes activities such as unpolarized target runs, target spin flip and target polarization measurements. Major target related down times can also be arranged together with the scheduled accelerator maintenance activities in order to reduce overhead time. This experiment will be run in parallel with already approved experiment E12-10-006, we share the 90 days of beam time with them.

Table 4: Beam time request.

	Time (Hour)	Time (Day)
Production on Pol. ^{3}He at 11 GeV	**1152**	48
Production on Pol. ^{3}He at 8.8 GeV	**576**	24
Dedicated Hydrogen run at 11 GeV	84	3.5
Dedicated Deuterium run at 11 GeV	84	3.5
Dedicated Hydrogen run at 8.8 GeV	36	1.5
Dedicated Deuterium run at 8.8 GeV	36	1.5
Other reference cell runs, optics and detector check	72	3.
Target Overhead: spin rotation, polarization measurement	120	5.
Total Time Request	**2160**	**90 days**

7 Summary

We are proposing a study of transversity parton distribution via measurements of semi-inclusive electroproduction of two charged pions from a transversely polarized ^{3}He (effective polarized neutron) target in DIS region with 11 and 8.8 GeV electron beam. The proposed experiment will use the approved SoLID spectrometer to provide precise SSA data in 4-D (x, Q^2, $M_{\pi^+\pi^-}$ and $z_{\pi^+\pi^-}$) space for the reaction of $^3\mathrm{He}^{\uparrow}(e, e'\pi^+\pi^-)\mathrm{X}$. The asymmetries on the neutron will be extracted after making correction for proton contribution and nuclear effects. The transversity distribution, h_1, will also be extracted. Combining these data with the results from a transversely polarized proton target in a similar x region measured by 12 GeV CLAS (PR12-12-009) or SoLID (E12-11-108) will provide a unique possibility to extract, in a model independent way, the u and d transversity distribution [67, 34]. It will also provide crucial input to calculate the tensor charge. Moreover, we propose to investigate a possible Sivers effect in dihadron SIDIS. This experiment will be run in parallel with already

approved experiment E12-10-006. A total number of 90 days of beam time will be shared by these two experiments.

References

[1] J. P. Ralston and D. E. Soper. Production of dimuons from high-energy polarized proton- proton collisions. *Nucl. Phys.*, B152:109, 1979.

[2] R. L. Jaffe and X. D. Ji. Chiral odd parton distributions and polarized drell-yan. *Phys. Rev. Lett.*, 67:552–555, 1991.

[3] J. Cortes, B. Pire, and J. Ralston. Measuring the transverse polarization of quarks in the proton. *Z.Phys.*, C55:409–416, 1992.

[4] X. Artru and M. Mekhfi. Transversely polarized parton densities, their evolution and their measurement. *Z. Phys.*, C45:669–676, 1990.

[5] M. Gockeler et al. Transverse spin structure of the nucleon from lattice QCD simulations. *Phys. Rev. Lett.*, 98:222001, 2007.

[6] V. Barone, A. Drago, and P. G. Ratcliffe. Transverse polarisation of quarks in hadrons. *Phys. Rept.*, 359:1–168, 2002.

[7] T. Bhattacharya, V. Cirigliano, S. D. Cohen, A. Filipuzzi, M. Gonzalez-Alonso, et al. Probing Novel Scalar and Tensor Interactions from (Ultra)Cold Neutrons to the LHC. *Phys.Rev.*, D85:054512, 2012.

[8] J. C. Collins. Fragmentation of transversely polarized quarks probed in transverse momentum distributions. *Nucl. Phys.*, B396:161–182, 1993.

[9] A. Airapetian et al. Effects of transversity in deep-inelastic scattering by polarized protons. *Phys. Lett.*, B693:11–16, 2010.

[10] M. Alekseev et al. Measurement of the Collins and Sivers asymmetries on transversely polarised protons. *Phys. Lett.*, B692:240–246, 2010.

[11] D. Boer, R. Jakob, and P. J. Mulders. Asymmetries in polarized hadron production in e^+e^- annihilation up to order 1/q. *Nucl. Phys.*, B504:345–380, 1997.

[12] K. Abe et al. Measurement of azimuthal asymmetries in inclusive production of hadron pairs in e^+e^- annihilation at Belle. *Phys. Rev. Lett.*, 96:232002, 2006.

[13] R. Seidl et al. Measurement of Azimuthal Asymmetries in Inclusive Production of Hadron Pairs in e^+e^- Annihilation at $\sqrt{s} = 10.58$ GeV. *Phys. Rev.*, D78:032011, 2008.

[14] M. Anselmino et al. Transversity and collins functions from sidis and e^+e^- data. *Phys. Rev.*, D75:054032, 2007.

[15] J. C. Collins and D. E. Soper. Back-to-back jets in qcd. *Nucl. Phys.*, B193:381, 1981.

[16] X. D. Ji, J. P. Ma, and F. Yuan. Qcd factorization for semi-inclusive deep-inelastic scattering at low transverse momentum. *Phys. Rev.*, D71:034005, 2005.

[17] D. Boer. Angular dependences in inclusive two-hadron production at BELLE. *Nucl. Phys.*, B806:23–67, 2009.

[18] M. Anselmino, M. Boglione, and S. Melis. A Strategy towards the extraction of the Sivers function with TMD evolution. *Phys.Rev.*, D86:014028, 2012.

[19] S. M. Aybat and T. C. Rogers. TMD Parton Distribution and Fragmentation Functions with QCD Evolution. *Phys. Rev.*, D83:114042, 2011.

[20] A. Bacchetta and A. Prokudin. Evolution of the helicity and transversity Transverse-Momentum-Dependent parton distributions. 2013.

[21] J. C. Collins, D. E. Soper, and G. Sterman. Factorization of hard processes in qcd. *Adv. Ser. Direct. High Energy Phys.*, 5:1–91, 1988.

[22] R. Brock et al. Handbook of perturbative QCD: Version 1.0. *Rev. Mod. Phys.*, 67:157–248, 1995.

[23] M. Radici, R. Jakob, and A. Bianconi. Accessing transversity with interference fragmentation functions. *Phys. Rev.*, D65:074031, 2002.

[24] A. V. Efremov, L. Mankiewicz, and N. A. Tornqvist. Jet handedness as a measure of quark and gluon polarization. *Phys. Lett.*, B284:394–400, 1992.

[25] J. C. Collins and G. A. Ladinsky. On $\pi-\pi$ correlations in polarized quark fragmentation using the linear sigma model. 1994.

[26] R. L. Jaffe, X. M. Jin, and J. Tang. Interference fragmentation functions and the nucleon's transversity. *Phys. Rev. Lett.*, 80:1166–1169, 1998.

[27] A. Bacchetta and M. Radici. Partial-wave analysis of two-hadron fragmentation functions. *Phys. Rev.*, D67:094002, 2003.

[28] A. Airapetian et al. Evidence for a Transverse Single-Spin Asymmetry in Leptoproduction of $\pi^+\pi^-$ Pairs. *JHEP*, 0806:017, 2008.

[29] C. Adolph et al. Transverse spin effects in hadron-pair production from semi-inclusive deep inelastic scattering. 2012.

[30] A. Vossen et al. Observation of transverse polarization asymmetries of charged pion pairs in e^+e^- annihilation near $\sqrt{s} = 10.58$ GeV. *Phys.Rev.Lett.*, 107:072004, 2011.

[31] X. Artru and J. C. Collins. Measuring transverse spin correlations by 4 particle correlations in $e^+e^- \to 2$ jets. *Z. Phys.*, C69:277–286, 1996.

[32] D. Boer, R. Jakob, and M. Radici. Interference fragmentation functions in electron positron annihilation. *Phys. Rev.*, D67:094003, 2003.

[33] A. Bacchetta, A. Courtoy, and M. Radici. First glances at the transversity parton distribution through dihadron fragmentation functions. *Phys.Rev.Lett.*, 107:012001, 2011.

[34] A. Bacchetta, A. Courtoy, and M. Radici. First extraction of valence transversities in a collinear framework. *JHEP*, 1303:119, 2013.

[35] M. G. Echevarria, A. Idilbi, and I. Scimemi. A Unified Treatment of the QCD Evolution of All (Un-)Polarized TMD Functions: Collins Function as a Study Case. 2014.

[36] X. Qian et al. Single Spin Asymmetries in Charged Pion Production from Semi-Inclusive Deep Inelastic Scattering on a Transversely Polarized ^{3}He Target. *Phys.Rev.Lett.*, 107:072003, 2011.

[37] R. Z. Yang. Transverse proton spin structure at PHENIX. *AIP Conf.Proc.*, 1182:569–572, 2009.

[38] E. Leader, A. V. Sidorov, and D. B. Stamenov. Determination of Polarized PDFs from a QCD Analysis of Inclusive and Semi-inclusive Deep Inelastic Scattering Data. *Phys.Rev.*, D82:114018, 2010.

[39] S. Scopetta. Neutron single spin asymmetries from semi-inclusive deep inelastic scattering off transversely polarized He-3. *Phys.Rev.*, D75:054005, 2007.

[40] S. Scopetta. The Neutron transversity from semi-inclusive DIS off He-3. *Few Body Syst.*, 44:75–78, 2008.

[41] W. Vogelsang and F. Yuan. Single-transverse spin asymmetries: From dis to hadronic collisions. *Phys. Rev.*, D72:054028, 2005.

[42] M. Anselmino et al. Comparing extractions of sivers functions. 2005.

[43] M. Anselmino et al. Sivers Effect for Pion and Kaon Production in Semi- Inclusive Deep Inelastic Scattering. *Eur. Phys. J.*, A39:89–100, 2009.

[44] S. Arnold, A. V. Efremov, K. Goeke, M. Schlegel, and P. Schweitzer. Sivers effect at Hermes, Compass and Clas12. 2008.

[45] A. Bacchetta and M. Radici. Constraining quark angular momentum through semi-inclusive measurements. *Phys.Rev.Lett.*, 107:212001, 2011.

[46] L. Kaptari, A. Del Dotto, E. Pace, G. Salme', and S. Scopetta. Distorted spin-dependent spectral function of an A=3 nucleus and semi-inclusive deep inelastic scattering processes. *Phys.Rev.*, C89:035206, 2014.

[47] C. Ciofi degli Atti and L. P. Kaptari. Semi-inclusive deep-inelastic scattering off few-nucleon systems: Tagging the emc effect and hadronization mechanisms with detection of slow recoiling nuclei. *Phys. Rev. C*, 83:044602, Apr 2011.

[48] A. Bacchetta, M. Diehl, K. Goeke, A. Metz, P. J. Mulders, and M. Schlegel. Semi-inclusive deep inelastic scattering at small transverse momentum. *JHEP*, 02:093, 2007.

[49] M. Diehl and S. Sapeta. On the analysis of lepton scattering on longitudinally or transversely polarized protons. *Eur. Phys. J.*, C41:515–533, 2005.

[50] A. Bacchetta, U. D'Alesio, M. Diehl, and C. A. Miller. Single-spin asymmetries: The trento conventions. *Phys. Rev.*, D70:117504, 2004.

[51] J. Zhou and A. Metz. Dihadron fragmentation functions for large invariant mass. *Phys.Rev.Lett.*, 106:172001, 2011.

[52] A. Bacchetta and M. Radici. Two-hadron semi-inclusive production including subleading twist. *Phys. Rev.*, D69:074026, 2004.

[53] A. Courtoy, A. Bacchetta, M. Radici, and A. Bianconi. First extraction of Interference Fragmentation Functions from e^+e^- data. *Phys.Rev.*, D85:114023, 2012.

[54] S. V. Gliske. *Transverse target moments of dihadron production in semi-inclusive deep inelastic scattering at HERMES*. PhD thesis, Michigan U., 2011. http://www-hermes.desy.de/notes/pub/11-LIB/sgliske.11-003.thesis.pdf.

[55] A. Bianconi, S. Boffi, R. Jakob, and M. Radici. Two-hadron interference fragmentation functions. ii: A model calculation. *Phys. Rev.*, D62:034009, 2000.

[56] A. Bacchetta and M. Radici. Modeling dihadron fragmentation functions. *Phys. Rev.*, D74:114007, 2006.

[57] A. Bacchetta, F. A. Ceccopieri, A. Mukherjee, and M. Radici. Asymmetries involving dihadron fragmentation functions: from DIS to e^+e^- annihilation. *Phys. Rev.*, D79:034029, 2009.

[58] A. Casey, H. H. Matevosyan, and A. W. Thomas. Calculating Dihadron Fragmentation Functions in the NJL-jet model. *Phys.Rev.*, D85:114049, 2012.

[59] H. H. Matevosyan, A. W. Thomas, and W. Bentz. Dihadron fragmentation functions within the NambuJona-Lasiniojet model. *Phys.Rev.*, D88(9):094022, 2013.

[60] H. H. Matevosyan, A. Kotzinian, and A. W. Thomas. Studies of Azimuthal Modulations in Two Hadron Fragmentation of a Transversely Polarised Quark. *Phys.Lett.*, B731:208–216, 2014.

[61] X. Artru and J. C. Collins. Measuring transverse spin correlations by 4 particle correlations in $e^+e^- \to 2$ jets. *Z.Phys.*, C69:277–286, 1996.

[62] R. L. Jaffe and X. D. Ji. Chiral odd parton distributions and drell-yan processes. *Nucl. Phys.*, B375:527–560, 1992.

[63] A. Hayashigaki, Y. Kanazawa, and Y. Koike. Next-to-leading order q**2 evolution of the transversity distribution h(1) (x, q**2). *Phys. Rev.*, D56:7350–7360, 1997.

[64] S. Kumano and M. Miyama. Two-loop anomalous dimensions for the structure function h_1. *Phys. Rev.*, D56:2504–2508, 1997.

[65] W. Vogelsang. Next-to-leading order evolution of transversity distributions and Soffer's inequality. *Phys. Rev.*, D57:1886–1894, 1998.

[66] M. Anselmino, M. Boglione, U. D'Alesio, A. Kotzinian, F. Murgia, A. Prokudin, and S. Melis. Update on transversity and Collins functions from SIDIS and e^+e^- data. *Nucl. Phys. Proc. Suppl.*, 191:98–107, 2009.

[67] M. Anselmino, M. Boglione, U. D'Alesio, S. Melis, F. Murgia, et al. Simultaneous extraction of transversity and Collins functions from new SIDIS and e+e- data. *Phys.Rev.*, D87:094019, 2013.

[68] G. R. Goldstein, J. O. G. Hernandez, and S. Liuti. Flavor dependence of chiral odd generalized parton distributions and the tensor charge from the analysis of combined π^0 and η exclusive electroproduction data. 2014.

[69] P. V. Pobylitsa and M. V. Polyakov. Transverse spin distribution function of nucleon in chiral theory. *Phys. Lett.*, B389:350–357, 1996.

[70] B. Q. Ma, I. Schmidt, and J. Soffer. The Quark spin distributions of the nucleon. *Phys.Lett.*, B441:461–467, 1998.

[71] R. Jakob, P. J. Mulders, and J. Rodrigues. Modelling quark distribution and fragmentation functions. *Nucl. Phys.*, A626:937–965, 1997.

[72] J. Soffer. Positivity constraints for spin dependent parton distributions. *Phys. Rev. Lett.*, 74:1292–1294, 1995.

[73] J. Soffer, M. Stratmann, and W. Vogelsang. Accessing transversity in double-spin asymmetries at the bnl-rhic. *Phys. Rev.*, D65:114024, 2002.

[74] V. A. Korotkov, W. D. Nowak, and K. A. Oganessyan. Transversity distribution and polarized fragmentation function from semi-inclusive pion electroproduction. *Eur. Phys. J.*, C18:639–644, 2001.

[75] P. Schweitzer et al. Transversity distributions in the nucleon in the large-n(c) limit. *Phys. Rev.*, D64:034013, 2001.

[76] M. Wakamatsu. Comparative analysis of the transversities and the longitudinally polarized distribution functions of the nucleon. *Phys. Lett.*, B653:398–403, 2007.

[77] B. Pasquini, M. Pincetti, and S. Boffi. Chiral-odd generalized parton distributions in constituent quark models. *Phys. Rev.*, D72:094029, 2005.

[78] I. C. Cloet, W. Bentz, and A. W. Thomas. Transversity quark distributions in a covariant quark- diquark model. *Phys. Lett.*, B659:214–220, 2008.

[79] A. Bacchetta, F. Conti, and M. Radici. Transverse-momentum distributions in a diquark spectator model. *Phys. Rev.*, D78:074010, 2008.

[80] C. Bourrely, F. Buccella, and J. Soffer. Semiinclusive DIS cross sections and spin asymmetries in the quantum statistical parton distributions approach. *Phys.Rev.*, D83:074008, 2011.

[81] H. He and X. D. Ji. The nucleon's tensor charge. *Phys. Rev.*, D52:2960–2963, 1995.

[82] B. Pasquini, M. Pincetti, and S. Boffi. Drell-Yan processes, transversity and light-cone wavefunctions. *Phys. Rev.*, D76:034020, 2007.

[83] L. P. Gamberg and G. R. Goldstein. Flavor spin symmetry estimate of the nucleon tensor charge. *Phys. Rev. Lett.*, 87:242001, 2001.

[84] M. Gockeler et al. Quark helicity flip generalized parton distributions from two-flavor lattice QCD. *Phys.Lett.*, B627:113–123, 2005.

[85] M. B. Hecht, C. D. Roberts, and S. M. Schmidt. Neutron electric dipole moment: Constituent dressing and compositeness. *Phys.Rev.*, C64:025204, 2001.

[86] C. Roberts. Private communication.

[87] J. Green, M. Engelhardt, S. Krieg, J. Negele, A. Pochinsky, et al. Nucleon Structure from Lattice QCD Using a Nearly Physical Pion Mass. 2012.

[88] T. Bhattacharya, S. D. Cohen, R. Gupta, A. Joseph, and H.-W. Lin. Nucleon Charges and Electromagnetic Form Factors from 2+1+1-Flavor Lattice QCD. *Phys.Rev.*, D89:094502, 2014.

[89] C. Bourrely, J. Soffer, and O. V. Teryaev. The q**2 evolution of soffer inequality. *Phys. Lett.*, B420:375–381, 1998.

[90] A. M. D., W. J. Stirling, R. S. Thorne, and G. Watt. Parton distributions for the LHC. *Eur. Phys. J.*, C63:189–285, 2009.

[91] D. de Florian, G. Navarro, and R. Sassot. Sea quark and gluon polarization in the nucleon at NLO accuracy. *Phys.Rev.*, D71:094018, 2005.

[92] A. Bacchetta, M. Radici, F. Conti, and M. Guagnelli. Weighted azimuthal asymmetries in a diquark spectator model. *Eur. Phys. J.*, A45:373–388, 2010.

[93] M. Radici. Unpolarized and Polarized Fragmentation Functions. 2011.

[94] J. C. Collins. Fragmentation of transversely polarized quarks probed in transverse momentum distributions. *Nucl.Phys.*, B396:161–182, 1993.

[95] P. J. Mulders and R. D. Tangerman. The complete tree-level result up to order $1/q$ for polarized deep-inelastic leptoproduction. *Nucl. Phys.*, B461:197–237, 1996. Erratum-ibid. **B484** (1997) 538.

[96] A. M. Kotzinian and P. J. Mulders. Probing transverse quark polarization via azimuthal asymmetries in leptoproduction. *Phys. Lett.*, B406:373–380, 1997.

[97] D. Boer and P. J. Mulders. Time-reversal odd distribution functions in leptoproduction. *Phys. Rev.*, D57:5780–5786, 1998.

[98] D. W. Sivers. Single Spin Production Asymmetries from the Hard Scattering of Point-Like Constituents. *Phys.Rev.*, D41:83, 1990.

[99] S. J. Brodsky, D. S. Hwang, and I. Schmidt. Final-state interactions and single-spin asymmetries in semi-inclusive deep inelastic scattering. *Phys. Lett.*, B530:99–107, 2002.

[100] S. J. Brodsky, P. Hoyer, N. Marchal, S. Peigne, and F. Sannino. Structure functions are not parton probabilities. *Phys.Rev.*, D65:114025, 2002.

[101] J. C. Collins. Leading twist single transverse-spin asymmetries: Drell-Yan and deep inelastic scattering. *Phys.Lett.*, B536:43–48, 2002.

[102] X. D. Ji and F. Yuan. Parton distributions in light-cone gauge: Where are the final-state interactions? *Phys. Lett.*, B543:66–72, 2002.

[103] A. V. Belitsky, X. D. Ji, and F. Yuan. Final state interactions and gauge invariant parton distributions. *Nucl. Phys.*, B656:165–198, 2003.

[104] M. Burkardt. Chromodynamic lensing and transverse single spin asymmetries. *Nucl. Phys.*, A735:185–199, 2004.

[105] S. Meissner, A. Metz, and K. Goeke. Relations between generalized and transverse momentum dependent parton distributions. *Phys. Rev.*, D76:034002, 2007.

[106] A. Kotzinian, H. H. Matevosyan, and A. W. Thomas. Sivers Effect in Two Hadron Electroproduction. 2014.

[107] A. Kotzinian, H. H. Matevosyan, and A. W. Thomas. Sivers Effect in Dihadron Semi-Inclusive Deep Inelastic Scattering. 2014.

[108] M. Anselmino et al. The role of cahn and sivers effects in deep inelastic scattering. *Phys. Rev.*, D71:074006, 2005.

[109] G. Ingelman, A. Edin, and J. Rathsman. LEPTO 6.5: A Monte Carlo generator for deep inelastic lepton - nucleon scattering. *Comput.Phys.Commun.*, 101:108–134, 1997.

[110] A. Kotzinian. Including Cahn and Sivers effects into event generators. pages 228–235, 2005.

[111] A. Kotzinian. Cahn and Sivers effects in the target fragmentation region of SIDIS. 2005.

[112] P. Souder et al. Precision measurement of parity-violation in deep inelastic scattering over a broad kinematic range. *JLab Experiment E12-10-007*, 2010.

[113] H. Gao et al. Target single spin asymmetry in semi-inclusive deep-inelastic $(e, e\pi^{\pm})$ reaction on a transversely polarized ^{3}he target at 8.8 and 11 gev. *JLab Experiment E12-10-006*, 2010.

[114] J. Huang et al. Asymmetries in semi-inclusive deep-inelastic $(e, e\pi^{\pm})$ reactions on a longitudinally polarized ^{3}he target at 8.8 and 11 gev. *JLab Experiment E12-11-007*, 2011.

[115] H. Gao et al. Target single spin asymmetry in semi-inclusive deep-inelastic $(e, e'\pi^{\pm})$ reaction on a transversely polarized proton target. *JLab Experiment E12-11-108*, 2012.

[116] Z. E. Meziani et al. Near threshold electroproduction of $j|\psi$ at 11 gev. *JLab Experiment E12-12-006*, 2012.

[117] J. Chen et al. Measurement of single target-spin asymmetry in semi-inclusive $n \uparrow (e, e'\pi^{-})$ reaction on a transversely polarized ^{3}he target. *JLab Experiment E06-110*, 2008.

[118] T. S. Collaboration. Solid preliminary conceptual design report. *Computer Physics Communications*, 2013.

[119] L. Mankiewicz, A. Schafer, and M. Veltri.
itPEPSI,a monte carlo generator for polarized leptoproduction. *Computer Physics Communications*, 71(3):305 – 318, 1992.